


ORIGINAL ARTICLE

Bacterial-like nitric oxide synthase in the haloalkaliphilic archaeon *Natronomonas pharaonis*

Silvia S. Orsini¹ | Kimberly L. James¹ | Destiny J. Reyes¹ | Ricardo L. Couto-Rodriguez¹ | Miriam K. Gulko² | Angela Witte³ | Ronan K. Carroll⁴ | Kelly C. Rice¹ 

¹Department of Microbiology and Cell Science, IFAS, University of Florida, Gainesville, FL, USA

²Department Oesterhelt, Max Planck Institut für Biochemie, Martinsried, Germany

³Department of Microbiology, Immunobiology and Genetics, MPL Laboratories, University of Vienna, Vienna, Austria

⁴Department of Biological Sciences, Ohio University, Athens, OH, USA

Correspondence

Kelly C. Rice, Department of Microbiology and Cell Science, IFAS, University of Florida, Gainesville, FL 32611-0700, USA. Email: kcrice@ufl.edu

Present address

Silvia S. Orsini and Destiny J. Reyes, Pharma Services, Viral Vector Services, Thermo Fisher Scientific, Alachua, FL, USA

Funding information

National Institute of Allergy and Infectious Diseases, Grant/Award Number: AI118999

Abstract

Bacterial nitric oxide (NO) synthases (bNOS) play diverse and important roles in microbial physiology, stress resistance, and virulence. Although bacterial and mammalian NOS enzymes have been well-characterized, comparatively little is known about the prevalence and function of NOS enzymes in Archaea. Analysis of archaeal genomes revealed that highly conserved bNOS homologs were restricted to members of the Halobacteria. Of these, *Natronomonas pharaonis* NOS (npNOS) was chosen for further characterization. NO production was confirmed in heterologously expressed His-tagged npNOS by coupling nitrite production from N-hydroxy-L-arginine in an H₂O₂-supported reaction. Additionally, the *nos* gene was successfully targeted and disrupted to create a *Nmn. pharaonis nos* mutant by adapting an established *Natrialba magadii* transformation protocol. Genome re-sequencing of this mutant revealed an additional frameshift in a putative cation-acetate symporter gene, which could contribute to altered acetate metabolism in the *nos* mutant. Inactivation of *Nmn. pharaonis nos* was also associated with several phenotypes congruent with bacterial *nos* mutants (altered growth, increased oxygen consumption, increased pigment, increased UV susceptibility), suggesting that NOS function may be conserved between bacteria and archaea. These studies are the first to describe genetic inactivation and characterization of a *Nmn. pharaonis* gene and provides enhanced tools for probing its physiology.

KEYWORDS

acetate, archaea, *Natronomonas pharaonis*, nitric oxide synthase, stress resistance

1 | INTRODUCTION

Nitric oxide (NO), a diffusible free radical gas, is involved in many biological functions, including cell signaling, stress mediation, cytotoxicity, and defense (Wink et al., 1996). Because of its reactive nature, NO can directly interact with cellular components including cysteine

thiols, heme cofactors, iron-sulfur clusters, lipids, and DNA, as well as oxygen and other reactive oxygen and reactive nitrogen species (ROS/RNS) (Czapski & Goldstein, 1995; Jourdeheuil et al., 1997; Lancaster, 1994; Wink et al., 1996). The primary route for NO production in mammalian cells is through nitric oxide synthase (NOS; EC 1.14.13.39) (Knowles & Moncada, 1994). NOS catalyzes a two-step reaction to

Silvia S. Orsini and Kimberly L. James contributed equally to this work.

This is an open access article under the terms of the Creative Commons Attribution-NonCommercial-NoDerivs License, which permits use and distribution in any medium, provided the original work is properly cited, the use is non-commercial and no modifications or adaptations are made.

© 2020 The Authors. *MicrobiologyOpen* published by John Wiley & Sons Ltd.

generate NO: In the first step, L-arginine is oxidized at its terminal (omega) guanidine nitrogen, resulting in the intermediate N(omega)-hydroxy-L-arginine (NOHA); in the second step, NOHA is oxidized releasing the terminal guanidine nitrogen as nitric oxide, with the generation of citrulline (Stuehr et al., 2004). Mammalian cells have three well-characterized isoforms of NOS (recently reviewed in Bogdan, 2015; Cinelli et al., 2019; Costa et al., 2016; Zhou & Zhu, 2009), two of which (neuronal NOS and endothelial NOS) participate in a wide variety of cell signaling processes, with the third isoform (inducible NOS; iNOS) an important component of immune cell oxidative burst.

Nitric oxide synthase homologs are also found in Gram-positive bacteria (Sudhamsu & Crane, 2009) such as *Bacillus*, *Staphylococcus*, *Deinococcus*, and *Streptomyces* (Bird et al., 2002; Johnson et al., 2008; Reece et al., 2009; Wang et al., 2007). These bacterial NOS (bNOS; EC 1.14.14.47) proteins are highly homologous to the oxygenase domain of mammalian NOS but lack the reductase domain that uses NADPH as reductant (Gusarov et al., 2008). Previous studies suggested that bNOS can promiscuously associate with various reductases in the cell (Gusarov et al., 2008; Wang et al., 2007). In *B. subtilis*, NOS-derived NO protects from oxidative stress caused by hydrogen peroxide (H_2O_2) by activating catalase (Gusarov & Nudler, 2005), while inactivation of *nos* in *S. aureus* leads to increased sensitivity to H_2O_2 despite an increase in catalase activity (Gusarov & Nudler, 2005; Mogen et al., 2017; Sapp et al., 2014). NOS-derived NO reduces antibiotic stress in *B. subtilis* and *S. aureus* (Gusarov et al., 2009; van Sorge et al., 2013), influences *B. anthracis* and *S. aureus* virulence (James et al., 2019; Popova et al., 2015; Sapp et al., 2014; van Sorge et al., 2013), modulates *S. aureus* cell respiration (Chaudhari et al., 2017; Kinkel et al., 2016; Mogen et al., 2017), regulates growth and recovery after exposure to ultraviolet and ionizing radiation, and affects carotenoid formation in *D. radiodurans* (Hansler et al., 2016; Patel et al., 2009).

A *nos* homolog was previously identified in the *Natronomonas pharaonis* genome (Gusarov et al., 2009; Sudhamsu & Crane, 2009), a haloalkaliphilic archaeon typically found in soda lakes (Gonzalez et al., 2010). Herein, we assess the prevalence of bNOS among archaeal genomes and characterize *Nmn. pharaonis* NOS (npNOS) using a combination of bioinformatic, genetic, and biochemical approaches. Our results suggest that NOS-like homologs sharing high amino acid identity to bNOS are restricted primarily to haloalkaliphilic archaea. Furthermore, recombinant npNOS produces NO, as assessed by measuring nitrite production from NOHA. A *Nmn. pharaonis nos* mutant was also generated and characterized using new and/or optimized tools for probing the physiology of this organism.

2 | MATERIALS AND METHODS

2.1 | Strains and culture conditions

A complete list of strains and plasmids used in this study is found in Table A1 in Appendix 1. *Escherichia coli* strains DH5 α and JM110 were used for plasmid construction and/or maintenance, whereas

strain BL21[(DE3)] was used for all protein expression studies. Antibiotics (ampicillin and kanamycin) for *E. coli* plasmid maintenance were used at 50 μ g/ml final concentration. *E. coli* strains were grown on lysogeny broth (LB) agar plates from glycerol stocks (25% v/v) and incubated at 37°C for 16–24 h. A single colony was inoculated into 3 ml of LB broth in a sterile 15-ml aerated culture tube and grown as specified below for npNOS or saNOS expression. These starter cultures were each used to inoculate 1-L LB medium containing 0.5% (w/v) glucose.

Natronomonas pharaonis DSM 2160 and isogenic *nos::gyrB* mutant (created in this study, see below) were used for all other experiments. NVM+medium was used for transformation and was prepared as described in (Haider, 2009) and Methods in Appendix 1. DSM 205, a casamino acid-based complex medium for growth of *Natronobacterium* described by the Leibniz Institute DSMZ-German Collection of Microorganisms and Cell Cultures (<https://www.dsmz.de/collection/catalogue/microorganisms/culture-technology/list-of-media-for-microorganisms>), was also used for indicated experiments and was prepared with modifications as described in Methods in Appendix 1 (referred to as “modified DSM 205”). *Nmn. pharaonis* was grown at 40°C and 250 rpm in a 1:5 volume-to-flask ratio (aerobically) unless otherwise stated. The recipe for the acetate minimal medium from (Gonzalez et al., 2010) was used for Bioscreen growth experiments. The *nos::gyrB* mutant was cultured with novobiocin (3–5 μ g/ml final concentration, depending on the experiment). For each experiment, *Nmn. pharaonis* glycerol stocks (20% v/v) were struck on NVM+or modified DSM 205 agar plates and incubated at 42°C for 5–10 days in plastic bags to minimize evaporation of plates. Starter cultures were inoculated by placing a loop-full of colonies into 10 ml of appropriate broth in a sterile 50 ml conical screw-top tube with the cap loosened and grown at 40°C and 250 rpm for 48–72 h. All experiments were performed using 10 ml starter cultures as the inoculum source for final media volumes adjusted as stated below for each experiment. Unless otherwise noted below, cultures were incubated at 40°C and 250 rpm.

2.2 | pET expression vector construction

All primers used in this study are listed in Table A2 in Appendix 1. The *N. pharaonis nos* gene was PCR amplified from genomic DNA with primer pair Npnos_NdeI_F/Npnos_NotI_R, and the *S. aureus nos* gene was amplified from strain UAMS-1 (Gillaspy et al., 1995) genomic DNA with primer pair Sanos_NdeI_F/Sanos_XhoI_R, using the Phusion High-Fidelity DNA Polymerase Kit. Each PCR product was ligated into pCR-Blunt (Thermo Fisher Scientific), transformed into *E. coli* DH5 α , and sequenced. The *Nmn.* and *S. aureus nos* inserts were then cut from pCR-Blunt with NdeI and NotI (*Nmn. nos*) or NdeI and XhoI (*S. aureus nos*), ligated into pET24b, and transformed into *E. coli* DH5 α . Plasmids containing inserts were sequenced before transformation into *E. coli* BL21(DE3) for protein purification.

2.3 | Protein purification

Escherichia coli BL21(DE3) containing pET24bnpNOS and pET24b-saNOS were each grown in LB supplemented with 5% (w/v) glucose in 1 L batches at 37°C until an OD₆₀₀ of 0.6 was reached; then, 100 µg/ml of γ -aminolevulinic acid was added. To induce the expression of npNOS, the pET24bnpNOS cultures were first incubated at 37°C shaking at 250 rpm to an OD₆₀₀ of 0.6, induced with 0.5 mM IPTG, and then shifted to an 18°C incubator and grown overnight with shaking at 250 rpm. To induce the expression of saNOS, the pET24bsaNOS cultures were incubated at 37°C shaking at 250 rpm, induced with 0.5 mM IPTG at an OD₆₀₀ of 0.6, and grown for 3–5 h 37°C shaking at 250 rpm. After growth, cells were harvested and lysed via FRENCH Press method (Thermo Electron Co). Expression of npNOS and saNOS was confirmed in the cytosolic and pellet fractions of the cell lysate, using SDS-PAGE and immunoblots with an anti-C-terminal His-tag primary mouse antibody (Invitrogen). Proteins were purified via nickel affinity chromatography and eluted at 100 mM imidazole. The purified fractions were buffer exchanged to remove imidazole by centrifuging samples (9000 g for 10 min) on 30-kDa centrifugal filters (Microcon) and exchanging the buffer 3 times with the following reaction buffers: npNOS buffer (50 mM HEPES, 3 M NaCl, pH 8) and saNOS buffer (50 mM HEPES, 500 mM NaCl, pH 8).

2.4 | Hydrogen peroxide (H₂O₂)-assisted NOS oxidation of N(omega)-hydroxy-L-arginine (NOHA)

Nitric oxide synthase activity of the recombinant proteins was validated through H₂O₂-assisted NOS oxidation of NOHA assay as first described in (Pufahl et al., 1995) and adapted from (Bird et al., 2002). One milliliter reactions were set up with 50 µl or 25 µl of NOS (either npNOS or saNOS), 10 units of superoxide dismutase, and 0.5 mM DTT. To begin the reaction, 50 µl of 10 mM NOHA and 3.4 µl of 30% H₂O₂ were added, and reactions were incubated at 37°C. At 3- and 30-min incubation, 250 µl was removed and stopped by the addition of 50 µl of catalase (1 mg/ml solution, from bovine liver, Sigma-Aldrich). Samples were then spun down at 15,000 g for 3 min and duplicate 100 µl volumes were aliquoted into a 96-well plate, where 50 µl of each Griess reagents 1 and 2 were added. Color was developed for 5 min, and absorbance at 548 nm was measured using a Biotek Synergy HT Plate Reader. All reactions performed in duplicate (2 × 50 µl reactions and 2 × 25 µl reactions). As negative controls, proteins were denatured with the addition of 6 µl of 100% (w/v) TCA to a 160 µl volume of each protein, and “no enzyme controls” were run with every set of samples.

2.5 | Creation of *nos::gyrB* mutant

The *Nmn. pharaonis nos* gene was amplified from genomic DNA with primers Npnos_EcoRI_F, and Npnos_HindIII_R, digested with EcoRI

and HindIII and ligated into pUC19 cut with the same enzymes (New England Biolabs) to generate pUC19-npnos. The novobiocin antibiotic resistance gene *gyrB* from plasmid pJAM809 (Humbard et al., 2009) was excised by BlnI and NsiI digestion, followed by Klenow treatment (New England Biolabs) to generate blunt ends. The *Nmn. nos* gene contains a naturally occurring NaeI site located 560-bp downstream of the ATG start codon. Since this restriction site is not present in the pUC19 sequence, digestion of pUC19-npnos with NaeI was performed to linearize the plasmid, followed by dephosphorylation with Antarctic Phosphatase and Klenow treatment to generate blunt ends. This linearized DNA was then ligated to blunt-ended *gyrB* and transformed into *E. coli* DH5 α to generate pUC19nos::*gyrB*. The orientation of the *gyrB* insertion in this plasmid was determined via Sanger sequencing. Plasmid pUC19nos::*gyrB* was then transformed into *E. coli* JM110, and plasmid was isolated in quantities of 20–30 µg for transformation into *Nmn. pharaonis*.

The *Nmn. pharaonis* transformation protocol was adapted from (Haider, 2009). *Nmn. pharaonis* cultures were grown at 37°C 250 rpm in 10 ml of modified DSM 205 containing 70 µg/ml of bacitracin in a 50 ml conical screw-cap tube to an OD₆₀₀ of 0.4–0.6 (about 3 days). Then, cells were centrifuged at 3900 g and resuspended with a half volume of buffered spheroplasting solution + glycerol containing 0.3 mg/ml of pronase E and incubated in a 42°C water bath for 48 h. At this point, 3 ml of cells was centrifuged at 10,000 g, resuspended in 150 µl of buffered spheroplasting solution–glycerol. 15 µl of EDTA pH 8.0 was carefully added to the cells, and the mixture was incubated for 10 min at room temperature. Linearized pUC19nos::*gyrB* DNA (cut with Scal digestion enzyme) was added afterward, and cells were incubated as described above for 5 min. Thereafter, 150 µl of PEG solution (60% (v/v) PEG 600 at 65°C and 40% (v/v) unbuffered spheroplasting solution) was carefully added to the cells. One milliliter of NVM+medium was added, and cells were subsequently centrifuged for 3 min. All supernatant was removed, and cells were resuspended in 1 ml of medium and recovered at 37°C shaking at 250 rpm for 2 days. Cells were plated on medium containing 5 µg/ml of novobiocin and incubated at 42°C. Once colonies appeared on plates, they were placed in culture tubes containing 4 ml of NVM+medium and 5 µg/ml of novobiocin and grown at 40°C, 250 rpm. Cells were re-cultured and diluted 1/10 in fresh medium containing novobiocin (5 µg/ml) every 3 days for a total of 15 passages. At passages 10 and 15, cells were plated on novobiocin (5 µg/ml) and individual colonies were screened for complete gene disruption (primers Npnos_promoter_F, *gyrB*_check_R, and Npnos_check_R) with primers flanking the cloning region. Several mutants lacking wild-type *nos* alleles were found at passage 15 and were stocked in glycerol, and one consistent isolate (A2) was used for further experiments.

2.6 | Growth curves

Wild-type and *nos::gyrB* mutant strains were streaked on modified DSM 205 medium (supplemented with 5 µg/ml novobiocin, as

necessary) and grown at 42°C for 5–6 days. A loop-full of colonies were used to inoculate a 50 ml conical tube containing 10 ml of media, and cultures were grown at 40°C and 250 rpm for about 2 days (to mid/late exponential growth phase). To measure initial OD₆₀₀ for inoculation, 500 µl of each culture was centrifuged at 14,000 g for 5 min to remove excess S-layer in the supernatant, and pellets were resuspended in a fresh sterile medium. This was found to give a more accurate measure of viable cells. Unless otherwise stated, cultures were inoculated to an OD₆₀₀ = 0.01 with each appropriate strain and grown in 50 ml of media in a 250 ml sterile foiled top Erlenmeyer flask (1:5 volume-to-flask ratio, 40°C, and 250 rpm). The OD₆₀₀, CFU/ml (via serial dilution plating), and pH measurements (using pH strips) were taken at 24-h intervals unless otherwise stated. For Bioscreen experiments, modified DSM 205 medium was amended with either 25 µM diethylenetriamine (DETA) or 25 µM DETA-NONOate to analyze the effect of an external source of NO, and acetate minimal media prepared according to (Gonzalez et al., 2010) was used to assess the ability of wild-type and *nos* mutant to utilize acetate as a carbon source for growth. From the overnight cultures, 10 ml of mid/late exponential-phase cultures was centrifuged at 4000 g and washed twice with growth medium. Bioscreen cultures were inoculated with washed cells to a target OD₆₀₀ = 0.02 and grown shaking at 42°C for chemical NO supplementation (Figure 2E), and a target OD₆₀₀ = 0.05 and 40°C for acetate consumption and modified DSM 205 growth curves (Figure 2D). The OD₆₀₀ was measured in 30 min or 3 h of increments for the duration of growth. To minimize evaporation, all exterior and interior wells not in use were filled with sterile H₂O. All Bioscreen cultures were grown in *n* = 2–5 biological replicates with four technical replicates for each culture.

2.7 | Quantification of extracellular acetate

Cultures were grown in modified DSM 205 medium as described above. One milliliter samples were taken at 0, 12, 24, 36, 48, 72, 96, 120, and 144 h of growth to determine extracellular acetate concentrations. Acetate was measured using an Acetic Acid Kit (R-Biopharm) that links acetyl-CoA and oxaloacetate to NAD⁺ reduction by citrate synthase and L-malate dehydrogenase. Procedures for measuring acetate were conducted according to the methods outlined in the R-Biopharm kit instruction manual, with an adjustment of the reaction volume to 283 µl. Assays were performed in 96-well culture plates (Costar 3596), and the absorbance at 340 nm was measured in a Cytation 3 Imaging Microplate Reader (BioTek). Each supernatant had *n* = 3 technical replicates and 2 biological replicates per strain per time point and modified DSM 205 medium was used to control for background.

2.8 | Pigment quantification via methanol extraction

Natronomonas pharaonis wild-type and *nos* mutant strains were grown in modified DSM 205 (complex medium) at 40°C and 250 rpm

for 120 h. At this point, 4.5 ml of each culture was centrifuged at 14,000 g for 5 min and then washed in 1 ml in Halo-HBSS (filter-sterilized Hank's balanced salt solution (Hanks & Wallace, 1949) without phenol red), supplemented with 3.5 M NaCl, and then adjusted to pH 8.5 with 6 N NaOH. Cells were resuspended in 1 ml of Halo-HBSS again and 100 µl was removed and added to 900 µl of sterile Halo-HBSS to determine OD₆₀₀ of cells for standardization. Cells were then centrifuged and resuspended in 650 µl of methanol. Cells were vortexed for at least 30 s and heated at 55°C for 5–10 min until cell debris became colorless. At this point, cells were centrifuged at 14,300 g for 3 min, and 600 µl of pigment-containing methanol was added to 400 µl of fresh methanol and the absorbance at both 490 and 525 nm was measured using a GENESYS 10 Bio Spectrophotometer (Thermo Scientific). Wild-type OD₆₀₀ was adjusted to 1.0, and all other sample ODs were adjusted to a relative OD ratio based on wildtype. The absorption for 490 nm and 525 nm was each normalized to the sample's respective relative OD ratio.

2.9 | DAF-FM diacetate staining

This assay was performed following protocols described in (Lewis et al., 2016) with slight modifications. Cultures were grown in modified DSM 205 medium, and at 24 h growth, a 5 ml aliquot was harvested by centrifugation at 3901 g for 10 min. Cells were resuspended in 1 ml Halo-HBSS with 10 µM DAF-FM diacetate and incubated statically at 37°C for 60 min. Cells were then pelleted (12,000 g for 5 min) and washed once in fresh Halo-HBSS. Cells were finally resuspended in 700–900 µl of Halo-HBSS to adjust for cell density differences, triplicate aliquots (200 µl) of stained cell suspensions were transferred to black optically clear-bottom 96-well plates (Costar 3904), and both OD₆₀₀ and fluorescence (relative fluorescent units, RFU) were measured as described in (Lewis et al., 2016) using a Biotek Synergy HT fluorescent plate reader.

2.10 | CTC staining

Respiration was measured using 5 mM 5-cyano-2,3-ditoly tetrazolium chloride (CTC) reduction, adapted from (Lewis et al., 2015; Mogen et al., 2017). Briefly, cultures were grown in modified DSM 205 medium at 40°C and 250 rpm as described above. At 24 h of growth, a culture volume equivalent to OD₆₀₀ = 1.0 from each strain was harvested by centrifugation at 3901 g for 10 min. Cells were washed once with 1 ml of Halo-HBSS and resuspended in 650 µl of Halo-HBSS with 5 mM CTC. Triplicate aliquots (200 µl) of stained cell suspensions were transferred to Costar 3904 plates. The plate was shaken 5 s before each read, and then, RFU (EX: 485 ± 20 nm, EM: 645 ± 40 nm) and OD₆₀₀ of each were measured at 10-min intervals at 37°C for 60 min using a Biotek Synergy HT Plate Reader. RFU collected at 30 min (the time point at which optimal fluorescence was measured, presented in Figure 4) was then normalized to the first (*t* = 0) OD₆₀₀ reading of each well.

2.11 | Oxygen consumption

Oxygen consumption was measured using a 4-Channel Free Radical Analyzer (TBR-4100, World Precision Instruments) and Clark-type electrode (ISO-Oxy-2, World Precision Instruments) with methods adapted from (Mogen et al., 2017). Exponential-phase cultures (24-h) growing aerobically in 100 ml (1:5 volume-to-flask ratio) of modified DSM 205 medium were harvested by centrifugation (3901 g, 22°C for 5 min), supernatant media was discarded, and pellets were resuspended in 700 µl of Halo-HBSS. The O₂ assay was conducted in a 20-ml disposable scintillation vial with 13 ml of Halo-HBSS buffer amended with 4 mM potassium acetate. The solution was stirred at 350 rpm and prewarmed to 40°C. O₂ consumption was measured for 25 min after the addition of 500 µl of the resuspended culture, and 2 ml of mineral oil overlay added to the vial to prevent oxygen equilibration from the atmosphere. The rate of O₂ loss for the *nos* mutant was determined using the slope O₂ decrease after 10 minutes incubation and normalized to wildtype. O₂ consumption rate was calculated by O₂ decrease after 10 minutes incubation normalized to OD₆₀₀ of resuspended culture (remaining 200 µl used).

2.12 | UV stress assay

Natronomonas pharaonis wild-type and *nos* mutant strains were grown in modified DSM 205 medium at 40°C and 250 rpm for 48 h in 50-ml conical screw-cap tubes, followed by sub-culturing to an OD₆₀₀ = 0.02 into 50-ml media in 250-ml sterile foil top Erlenmeyer flasks. Cultures were then incubated for an additional 48 hours, followed by centrifugation at 4000 g at 20°C for 10 min. Cells were resuspended in Halo-HBSS to an OD₆₀₀ = 0.4–0.5, and the volume of each culture was split into two square plastic Petri dishes. One plate was exposed to 750 mJ/cm² UV in HL-2000 HybriLinker Hybridization Oven/ UV Crosslinker (UVP), and the other plate was the untreated control. After UV exposure, cultures were transferred to 125 ml sterile foiled Erlenmeyer flasks and diluted 1:2 with modified DSM 205 medium. Flasks were incubated and recovered under light at 40°C and 250 rpm, and CFU/ml via serial dilution was measured at *t* = 0, 1, 3, 6, and 24 h. Data are expressed as percent survival between the untreated and UV treated samples for each strain at each time point.

2.13 | Statistical analysis

All quantitative data were analyzed for statistical significance using SigmaPlot software version 14, build 14.0.3.192 (Systat Software Inc.). Data were tested for normality and equal variance before choosing the appropriate parametric or non-parametric test, respectively.

3 | RESULTS AND DISCUSSION

3.1 | *Nmn. pharaonis* NP_1908A encodes a predicted bacterial NOS-like protein

The *S. aureus* MRSA252 *nos* open reading frame (GenPept accession# CAG40992) was used to tBLASTn search the NCBI RefSeq genome database, restricting the search to Archaea (TAXID 2157). This analysis yielded 15 hits (Table A3 in Appendix 1) with extensive query coverage (94%–98%), and a high degree of amino acid (AA) identity to *S. aureus* NOS (saNOS; 45%–51%). All identified NOS-containing genomes belonged to the Halobacteria class. Of these, 8 belonged to the Natribaceae, 5 to the Halobacteriales, and 2 to the Haloferacales. Interestingly, proteins with high AA identity to saNOS were not identified in methanogen or Crenarchaeota genomes in this analysis. Clustal-Omega AA alignment (Sievers et al., 2011) of a subset of these archaeal NOS homologs to saNOS and *B. subtilis* NOS (bsNOS) indicated high conservation of most active site, heme-binding and dimerization residues (Figure A1 in Appendix 1). At *B. subtilis* isoleucine 218, *Nmn. pharaonis* and most other Halobacteria NOS contain a valine, which is conserved in eukaryotic NOS proteins (Pant et al., 2002; Wang et al., 2004). This switch has been previously characterized in the context of *B. subtilis* NOS (bsNOS) and mammalian iNOS: When bsNOS was mutated I218V, the transition state of the heme was directly affected, while the mutation of iNOS V346I had a decrease in the dissociation rates of NO (Wang et al., 2004; Weisslocker-Schaetzel et al., 2017). Although the occupation of isoleucine versus valine at this conserved domain appears to play a role in NOS enzyme kinetics, this residue is not conserved among all potential *nos* homologs from archaeal genomes: *Nbt. gregoryi* contains the bacterial-like isoleucine, while most other archaeal NOS homologs (including *Nmn. pharaonis*) contain valine at this AA position (Figure A1 in Appendix 1).

3.2 | Demonstration of in vitro recombinant npNOS activity

To verify its gene function, npNOS (RefSeq locus tag NP_RS04750, original locus tag NP_1908A) and saNOS (RefSeq locus tag SAR_RS10475, original locus tag SAR2007) as a control were both heterologously expressed and purified from *E. coli*. NO production by each purified recombinant protein was measured using a H₂O₂-assisted NOHA oxidation assay (Pufahl et al., 1995), as previously described for saNOS and other NOS enzymes (Bird et al., 2002; Montgomery et al., 2010). In this assay, the NOS enzyme catalyzes the oxidation of N(omega)-hydroxy-L-arginine (NOHA) to NO, with H₂O₂ providing electrons instead of a redox partner. NO production by NOS is coupled to nitrite formation, that is, subsequently quantified using the Griess reagent. The saNOS and npNOS proteins produced 72.07 ± 26 and 77.35 ± 19 µmol nitrite min⁻¹ mg⁻¹, respectively.

These results confirm that npNOS catalyzes NO production in an in vitro assay at a comparable catalytic rate to the well-characterized saNOS (Bird et al., 2002), which suggests its physiological function may also be similar.

3.3 | Generation of a *Nmn. pharaonis* nos mutant

To further investigate the physiological role of the NP_1908A gene (henceforth referred to as *nos*; Figure 1A), we generated a *Nmn. pharaonis* *nos* mutant through gene disruption, in which the *Nmn. nos* gene sequence interrupted with a novobiocin resistance gene (*nos::gyrB*) was cloned into a suicide plasmid and subsequently introduced into *Nmn. pharaonis* using a modified transformation protocol (Figure 1B) (Derntl et al., 2015). A representative double-cross-over clone which demonstrated a mixture of wild-type and *nos::gyrB* alleles by PCR was then sub-cultured for ≥ 15 passages, yielding several colonies that completely lost the *nos* wild-type allele. Mutant A2 (*nos::gyrB*; Figure 1C) was chosen for further experiments.

Several attempts were made to complement the *nos::gyrB* mutant with cloning vector pRO5 developed for *Natrialba magadii* (Mayrhofer-Iro et al., 2013) modified to replace novobiocin selection with a mevinolin resistance cassette and containing the *Nmn. nos* gene and upstream promoter region. However, transformation

efforts were not successful in either the wild-type or mutant strains, highlighting the complexity of transforming haloalkaliphilic archaea. In the absence of a genetic counterselection system, the *Nmn. nos::gyrB* mutant had to be sub-passaged 15 times to completely lose the *nos* wild-type allele after the original integration event of the *nos::gyrB* allele into its genome. This sub-passaging step was necessary since *Nmn. pharaonis*, like many other halophilic archaea, is polyploid (Breuert et al., 2006). This, combined with our inability to perform genetic complementation of the *nos::gyrB* mutant, prompted our re-sequencing of the genomes of both wild-type and *nos::gyrB* mutant, which were analyzed for single nucleotide polymorphisms (SNPs) (Table A4 in Appendix 1), comparing each to the *Nmn. pharaonis* DSM 2160 reference genome (NC_007426.1). This analysis revealed that both the wild-type and *nos::gyrB* mutant shared eleven identical SNPs in coding regions that were distinct from the published genome sequence (Table A4 in Appendix 1). Additionally, the *nos::gyrB* mutant contained three SNPs that were not detected in the re-sequenced wild-type genome (Table A4 in Appendix 1): A P16S substitution in a predicted restriction endonuclease (NP_RS00005), a stop codon at position 23 in a predicted CheY response regulator (NP_RS05195), and a frameshift mutation at A227 in NP_RS12645 (NP_5136A), which bears 60–82% amino acid identity to proteins annotated as cation acetate symporters in several halophilic archaea. The observed accumulation of genomic

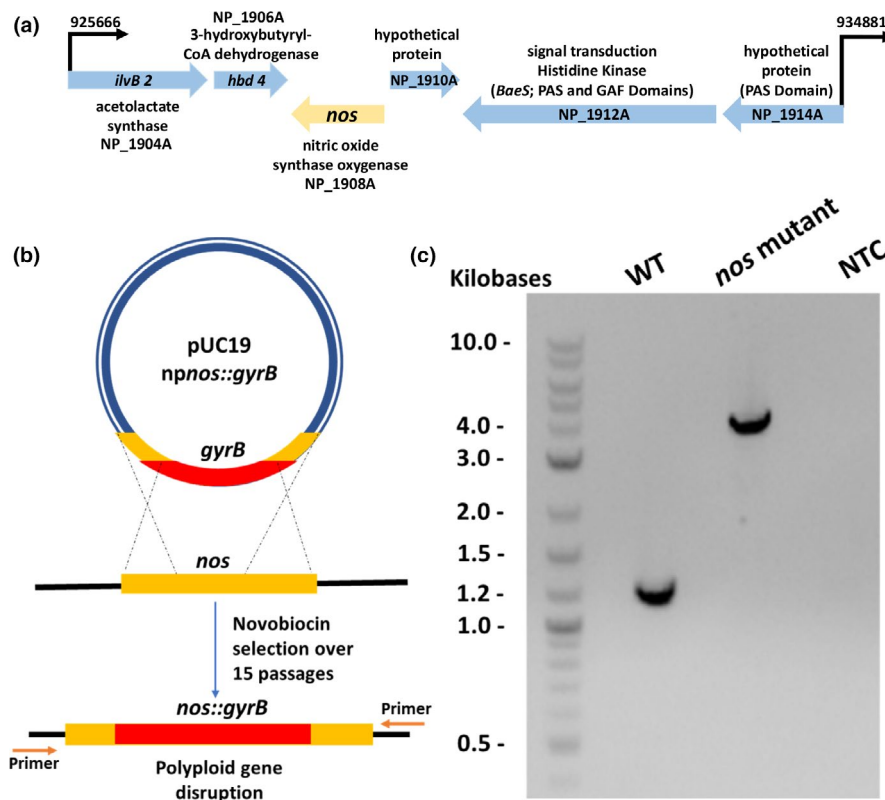


FIGURE 1 Disruption of *Nmn. pharaonis* *nos* gene. (A) Genomic organization surrounding *nos* (NP_1908A) in *Nmn. pharaonis*. (B) Schematic representation of the *nos* gene disruption by novobiocin resistance (*gyrB*) and mutant creation via homologous recombination. (C) Gel electrophoresis of PCR performed on wild-type and *nos* mutant genomic DNA using primers flanking the *nos* gene (annealing outside of the *nos::gyrB* allele). NTC = no template control.

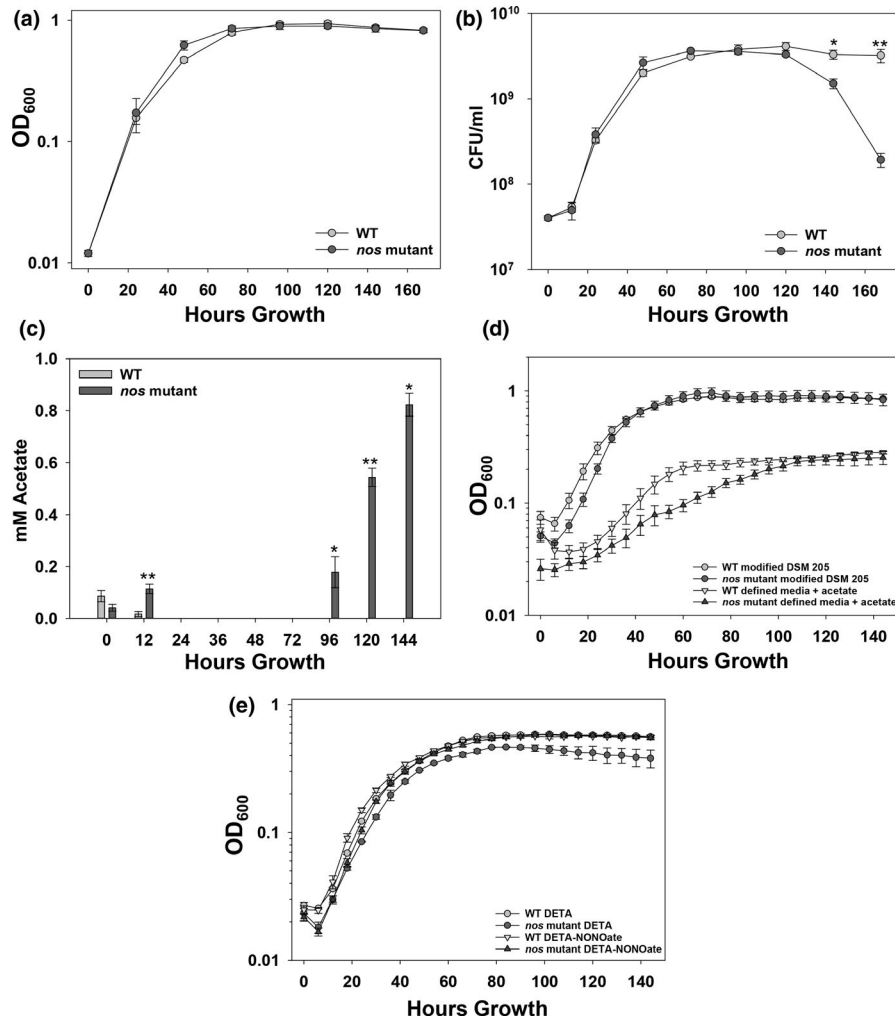


FIGURE 2 Growth curves of *Nmn. pharaonis* wild-type (WT) and *nos::gyrB* mutant cultures. (A, B) *Nmn. pharaonis* WT and *nos* mutant cultures were grown in modified DSM medium at 40°C, 250 RPM. Growth was monitored by OD₆₀₀ (A) and CFU ml⁻¹ (B). Data in A-B represent *n* = 4 experiments, error bars = SEM. **p* < 0.05 Welch's t test, ***p* < 0.01 Student's t test at each time point. (C) Supernatant levels of acetate from WT and *nos::gyrB* mutant growth curves were measured using an R-Biopharm Acetic Acid UV-method Kit. Data represent *n* = 2 biological replicates and 3 technical replicates. Error bars = SEM, **p* < 0.05 Mann-Whitney rank-sum test, ***p* < 0.01, Student's t test at each time point. (D) Growth curves performed at 40°C using a Bioscreen C to compare WT and *nos::gyrB* mutant growth in modified DSM 205 medium and minimal medium +acetate as a carbon source. Data represent *n* = 3 biological replicates, error bars = SEM. (E) Growth curves performed at 42°C using a Bioscreen C to compare WT and *nos::gyrB* mutant growth in modified DSM 205 medium supplemented with 25 μM DETA-NONOate or 25 μM DETA alone. Data represent *n* = 2 (*nos::gyrB* mutant DETA), *n* = 3 (WT DETA and WT DETA-NONOate), and *n* = 5 (*nos::gyrB* mutant DETA-NONOate) biological replicates, error bars = SEM.

SNPs in the *Nmn. nos::gyrB* mutant highlights the need for the development of future tools for *Nmn.* genetic manipulation that are similar in strategy to the *pyrE(F)*-positive selection/counterselection systems for mutant generation in *Haloferax* species (Bitan-Banin et al., 2003; Liu et al., 2011), or possibly CRISPR-based gene silencing as recently described for *Hfx. volcanii* (Stachler & Marchfelder, 2016).

3.4 | Growth and physiological differences observed in the *nos::gyrB* mutant

When grown aerobically in shaking flasks using modified DSM 205 (a complex casamino acid-based medium), a slight increase in mid-late

exponential-phase growth was observed in the *nos::gyrB* mutant (Figure 2A,B). Additionally, a significant reduction in viable cells (as assessed by CFU/ml) during late-stationary phase was observed in the *nos::gyrB* mutant but not in the wildtype, starting just after 120 hours growth (Figure 2B). Because of the A227 frameshift mutation identified in the NP_RS12645 (NP_5136A) gene (predicted cation acetate symporter; Table A4 in Appendix 1) of the *nos::gyrB* mutant, extracellular acetate levels during growth were also compared between wild-type and mutant strains. During early exponential growth, acetate was present in both wild type and mutant, albeit at low concentrations, and disappeared by mid-exponential growth phase (Figure 2C). However, the *nos::gyrB* mutant accumulated acetate throughout stationary phase (96–144 h growth), whereas

acetate was undetectable in the wildtype (Figure 2C). Since there was very little acetate detected in the medium at the time of inoculation (<0.1 mM), it is possible that the extracellular acetate detected in stationary phase *nos::gyrB* mutant cultures was due to increased acetate excretion (due to overflow metabolism) and/or an inability to reuptake excreted acetate due to the SNP mutation in the NP_5136A, a putative cation/acetate symporter. Interestingly, *Nmn. pharaonis* can sustain growth using acetate as a sole carbon source (Falb et al., 2005; Gonzalez et al., 2010). Comparison of growth in a Bioscreen C shaking microplate system in minimal medium (Gonzalez et al., 2010) with acetate as the sole carbon source (Figure 2D) revealed that the *nos::gyrB* mutant growth on acetate was overall reduced throughout exponential and early stationary growth phases compared to wildtype. This correlated with a decrease in maximum specific growth rate on acetate for the *nos::gyrB* mutant (0.029 ± 0.001 per hour) compared to wildtype (0.045 ± 0.004 per hour). Although these data suggest that growth is reduced in the *nos::gyrB* mutant when utilizing acetate as a carbon source, it is unclear whether this phenotype is specifically due to disruption of *nos*, and/or a result of the SNP detected in NP_5136A.

Interestingly, *nos::gyrB* mutant cultures grew better during exponential growth in Erlenmeyer flasks (Figure 2A,B), compared to growth in the Bioscreen (Figure 2D) relative to wild type when grown in modified DSM 205 medium. This may be due to altered aeration between the two growth methods (Biesta-Peters et al., 2010; Duetz & Witholt, 2004) and/or due to a slightly larger starter inoculum used in the Bioscreen experiment. To further characterize the effect of NO on the growth of the wildtype and *nos::gyrB* mutant, Bioscreen cultures were grown in modified DSM 205 with either the chemical NO donor DETA-NONOate or DETA alone (control) (Figure 2E). The OD_{600} of the *nos::gyrB* mutant at the experimental endpoint was approximately 1.5-fold higher in the presence of NO donor relative to the DETA control, whereas a comparable increase was not observed in the wild-type strain. NO donor improved exponential-phase growth of both the wildtype and *nos::gyrB* mutant, but this effect was more pronounced in the *nos::gyrB* mutant, restoring its maximum specific growth rate from 0.072 ± 0 per hour (with DETA alone) to 0.107 ± 0.002 per hour (with NO donor), representing a ~1.49-fold

increase. In comparison, the wild-type strain had a maximum specific growth rate of 0.108 ± 0.005 per hour in the DETA alone control culture, and 0.124 ± 0.007 per hour in the presence of NO donor, representing a ~1.15-fold increase.

It was also consistently observed in both flask-based and Bioscreen cultures that the *nos::gyrB* mutant visually displayed altered pigmentation relative to the wild type (Figure 3A). Pigment accumulation was therefore quantified using methanol-extracted pigments from cell samples collected from wild-type and mutant cultures at 120 h growth. Initial spectral analysis from 340–600 nm revealed peaks at 490 and 525 nm in both sets of cultures; however, the *nos::gyrB* mutant showed increased absorbance values at both of these wavelengths (Figure 3B). These peaks may reflect differences in bacterioruberin (525 nm) and/or its upstream precursor phytofluene (490 and 525 nm) (Ekiel et al., 1986; Falb et al., 2008). While bacterioruberin is well known in *Nmn. pharaonis* as it forms a complex with the light-driven ion pump halorhodopsin (Sasaki et al., 2012), it can also serve as an antioxidant to protect halophiles from oxidative damage (Miller et al., 1996) and can reinforce membrane rigidity (Lazrak et al., 1988; Rodrigo-Baños et al., 2015). Mutation of bacterial *nos* has also been shown to impact cell membrane-associated carotenoid levels in *S. aureus* (Sapp et al., 2014), *Staphylococcus xylosum* (Ras et al., 2017) and *D. radiodurans* (Hansler et al., 2016).

3.5 | Mutation of *nos* impacts *Nmn. pharaonis* intracellular RNS levels, cell respiration and stress resistance

Assessment of endogenous NO, respiratory, and stress resistance phenotypes were all performed in mid-late exponential-phase (24–48 h growth) shaking flask cultures. DAF-FM diacetate reacts with NO and/or other reactive nitrogen species (RNS) to form a fluorescent benzotriazole and was previously used to determine intracellular NO/RNS levels in *S. aureus* (Lewis et al., 2016; Sapp et al., 2014). DAF-FM diacetate staining was adapted here for use with *Nmn. pharaonis*. To first verify that DAF-FM diacetate was taken up by archaeal cells and responds to NO/RNS, exponential-phase

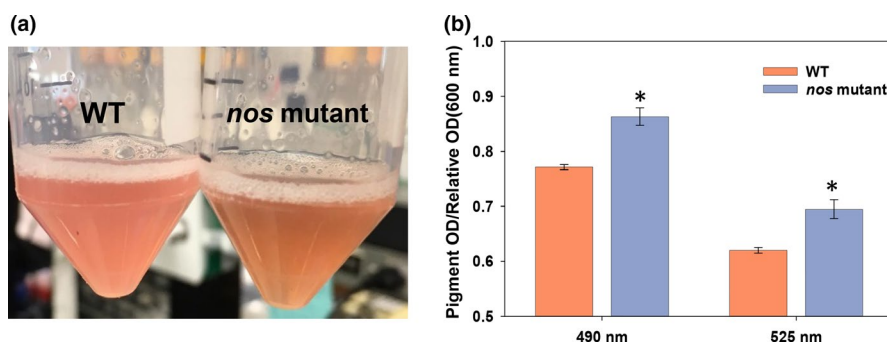
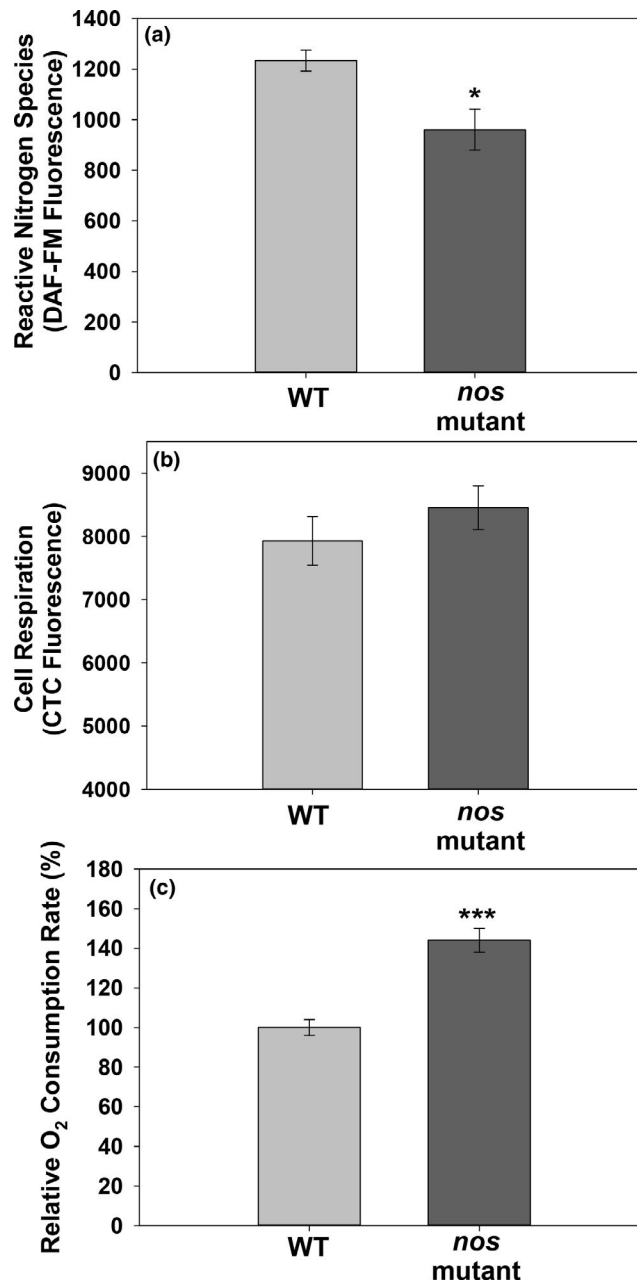


FIGURE 3 *Nmn. pharaonis nos::gyrB* mutant displays altered pigment. (A) Representative photograph of *Nmn. pharaonis* wild-type and *nos::gyrB* mutant aerobic cultures grown in modified DSM 205 medium. (B) Strains were grown in modified DSM 205 medium in shaking flasks as described for Figure 1A–B, and at 120-hour growth, the cell-associated pigment was extracted with methanol and quantified. $n = 3$ independent experiments. Error bars = SEM. * $p < 0.05$, Student's *t* test.

FIGURE 4 *Nmn. nos::gyrB* mutant exponential-phase cultures have altered respiration and reduced intracellular NO/RNS levels relative to wildtype. (A) Intracellular reactive nitrogen species (RNS) were detected in *Nmn. pharaonis* WT and *nos::gyrB* mutant cells at 24 hours growth by staining with 10 μ M DAF-FM diacetate. DAF-FM fluorescence is reported as relative fluorescent units (RFU) per OD₆₀₀ of each sample. Data represent the average of $n = 4$ independent experiments. Error bars = SEM. * $p < 0.05$, Student's t test. (B) Cellular respiration was detected in *Nmn. pharaonis* WT and *nos::gyrB* mutant cells at 24-hour growth by staining with 5 mM CTC. Fluorescence is reported as RFU per OD₆₀₀ of each sample. Data represent the average of $n = 3$ independent experiments, error bars = SEM. (C) Oxygen consumption of *Nmn. pharaonis* WT and *nos::gyrB* mutant was measured at exponential phase (24-hour growth) using a Clark-type electrode, normalized to the OD₆₀₀ of resuspended culture, and expressed as a percentage normalized to the wild-type oxygen consumption rate. Data represent the average of $n = 6$ independent experiments. Error bars = SEM. *** $p < 0.001$, Student's t test.

Haloferax volcanii and *Nmn. pharaonis* cells were each stained with 5 μ M DAF-FM diacetate, followed by incubation in the presence and absence of DEA-NONOate, a short half-life chemical NO donor. As expected, cells exposed to NO donor had higher DAF-FM fluorescence relative to the control DAF-FM cells (Figure A2 in Appendix 1). The concentration of DAF-FM diacetate was subsequently increased to 10 μ M to detect differences in endogenous NO/RNS in mid-exponential cells of wildtype and the *nos::gyrB* mutant, revealing a modest but statistically significant ($p < 0.05$, t test) reduction in DAF-FM fluorescence in the *nos::gyrB* mutant relative to wildtype (Figure 4A). Other cellular sources of NO and/or RNS may contribute to the DAF-FM fluorescence observed in the *nos::gyrB* mutant. A similar pattern of DAF-FM fluorescence was previously observed when assessing endogenous NO/RNS levels with DAF-FM in *S. aureus* wild-type and *nos* mutant cells (Sapp et al., 2014).

To evaluate whether disruption of the *Nmn. pharaonis nos* gene alters respiration, as was described previously for *S. aureus nos* mutants (Chaudhari et al., 2017; James et al., 2019; Kinkel et al., 2016; Mogen et al., 2017), *Nmn.* wild-type and *nos::gyrB* mutant cells were stained with 5 mM 5-cyano-2,3-ditolyl tetrazolium chloride (CTC) that acts as a redox partner for respiratory dehydrogenases. When CTC is reduced, it forms an insoluble fluorescent formazan complex that can be used as an indicator of cellular respiration (Bartosch et al., 2003; Créach et al., 2003; Smith & McFeters, 1996). Increased CTC staining in the *nos::gyrB* mutant observed at mid-exponential phase, although not statistically significant, suggested that respiration may be altered in this strain (Figure 4B). O₂ consumption of mid-exponential-phase cells was also measured using a Clark-type electrode (Figure 4C). Exponential-phase *Nmn. pharaonis nos::gyrB* mutant cultures consumed O₂ at a significantly higher rate ($p < 0.001$) than the wildtype (Figure 4C). These respiratory phenotypes mimic what was previously observed in three studies that showed *S. aureus nos* mutants had accelerated oxygen consumption during aerobic respiratory growth (James et al., 2019; Kinkel et al.,



2016; Mogen et al., 2017). Taken together, these data suggest that archaeal and bacterial NOS enzymes may share conserved functions in cellular respiration.

Halophilic archaea are exposed to strong levels of ultraviolet (UV) radiation in their natural environments [reviewed in (Jones & Baxter, 2017)]. Since UV stress resistance has been reported to be decreased in *Deinococcus radiodurans nos* mutants (Hansler et al., 2016; Patel et al., 2009), it is plausible that UV stress could have a more negative outcome for the *Nmn. pharaonis* in the absence of npNOS. *Nmn.* wildtype and *nos::gyrB* mutant were therefore assessed for viability and recovery when treated with 750 \times 100 μ J/cm² of ultraviolet light (UV). In this assay, the *Nmn. nos::gyrB* mutant had significantly ($p < 0.05$) reduced survival rates immediately after UV treatment compared to wild type (Figure 5), with both strains

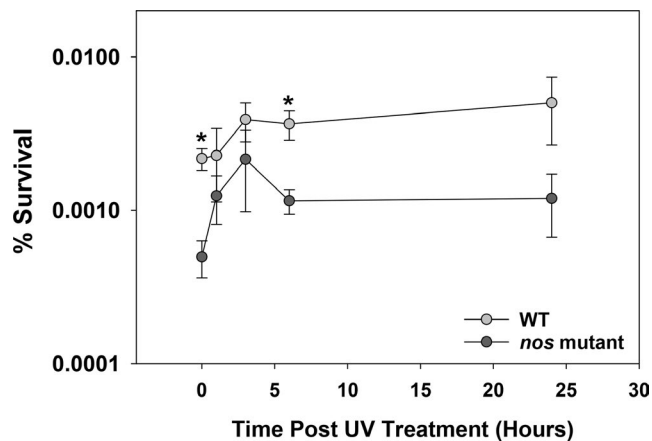


FIGURE 5 *Nmn. nos::gyrB* mutant displays reduced UV stress resistance. 48-hour cultures were split and treated with either $750 \times 100 \mu\text{J cm}^{-2}$ UV or no treatment, then recovered and plated. Data represented as percent survival of CFU ml^{-1} of treated to untreated cultures at each time point, $n = 3$ independent experiments. Error bars = SEM. * $p < 0.05$, Student's *t* test comparing WT to *nos::gyrB* mutant at each time point.

displaying only a small amount of recovery in viability throughout the 24 hour period following initial UV exposure. Increased UV susceptibility has also been demonstrated in *D. radiodurans nos* mutants, and while this was complemented both genetically and by supplementation with chemical NO donors, the exact mechanism remains unknown (Hansler et al., 2016; Patel et al., 2009).

4 | CONCLUSIONS

In this study, bioinformatic and biochemical approaches have confirmed that *Nmn. pharaonis* ORF NP_1908A encodes a bacterial-like NOS protein which can catalyze NO production from NOHA. Furthermore, *Nmn. pharaonis* NOS and/or its derived NO appears to serve a similar function to its bacterial counterpart with respect to protection against UV resistance, as the *Nmn. pharaonis nos::gyrB* mutant displayed decreased viability following UV exposure. Moreover, NOS and/or derived NO modulates aerobic respiration in *S. aureus* (Chaudhari et al., 2017; Kinkel et al., 2016; Mogen et al., 2017), and also appears to play a role in *Nmn. pharaonis* aerobic respiration, as the *nos::gyrB* mutant experienced increased rates of oxygen-based respiration. Successful genetic manipulation of *Nmn. pharaonis* as described herein opens many avenues for further investigation into its unique physiology necessary to thrive in extreme haloalkaliphilic environments.

ACKNOWLEDGMENTS

The authors gratefully acknowledge Dr Julie Maupin-Furlow and Dr Graciela Lorca (University of Florida, Department of Microbiology and Cell Science) for plasmids, strains, and technical advice. This work was supported in part by NIH grant AI118999 to KCR,

UF-IFAS Mid-Career International Travel Award to KCR, and Florida Education Fund McKnight Doctoral Fellowship to SSO.

CONFLICT OF INTEREST

None declared.

AUTHOR CONTRIBUTIONS

Silvia S Orsini: Conceptualization (equal); Formal analysis (equal); Funding acquisition (supporting); Investigation (equal); Methodology (equal); Writing-original draft (equal); Writing-review & editing (supporting). **Kimberly L James:** Conceptualization (supporting); Formal analysis (equal); Investigation (equal); Methodology (equal); Validation (equal); Writing-original draft (equal); Writing-review & editing (equal). **Destiny J Reyes:** Formal analysis (supporting); Investigation (supporting); Methodology (supporting); Writing-original draft (supporting); Writing-review & editing (supporting). **Ricardo L Couto-Rodriguez:** Formal analysis (supporting); Investigation (supporting); Methodology (supporting); Writing-original draft (supporting); Writing-review & editing (supporting). **Miriam Kolog Gulko:** Methodology (supporting); Writing-original draft (supporting). **Angela Witte:** Methodology (supporting); Resources (supporting); Writing-original draft (supporting); Writing-review & editing (supporting). **Ronan K Carroll:** Data curation (equal); Formal analysis (equal); Writing-original draft (supporting); Writing-review & editing (supporting). **Kelly C Rice:** Conceptualization (equal); Data curation (equal); Funding acquisition (lead); Project administration (lead); Writing-original draft (equal); Writing-review & editing (equal).

ETHICS STATEMENT

None required.

DATA AVAILABILITY STATEMENT

All data in this manuscript are included as figures or in the Appendix. All DNA raw sequencing data files have been deposited to the National Center for Biotechnology Information's Sequence Read Archive (SRA), under BioProject PRJNA630572: <https://www.ncbi.nlm.nih.gov/bioproject/PRJNA630572>.

ORCID

Kelly C. Rice  <https://orcid.org/0000-0003-1335-4409>

REFERENCES

- Alderton, W. K., Cooper, C. E., & Knowles, R. G. (2001). Nitric oxide synthases: structure, function and inhibition. *Biochemical Journal*, 357, 593–615.
- Allers, T., Ngo, H. P., Mevarech, M., & Lloyd, R. G. (2004). Development of additional selectable markers for the halophilic archaeon *Haloferax volcanii* based on the *leuB* and *trpA* genes. *Applied and Environmental Microbiology*, 70(2), 943–953. <https://doi.org/10.1128/aem.70.2.943-953.2004>
- Altschul, S. F., Gish, W., Miller, W., Myers, E. W., & Lipman, D. J. (1990). Basic local alignment search tool. *Journal of Molecular Biology*, 215, 403–410.

- Bartosch, S., Mansch, R., Knötzsch, K., & Bock, E. (2003). CTC staining and counting of actively respiring bacteria in natural stone using confocal laser scanning microscopy. *Journal of Microbiol Methods*, 52(1), 75–84.
- Biesta-Peters, E. G., Reij, M. W., Joosten, H., Gorris, L. G., & Zwietering, M. H. (2010). Comparison of two optical-density-based methods and a plate count method for estimation of growth parameters of *Bacillus cereus*. *Applied and Environment Microbiology*, 76(5), 1399–1405. <https://doi.org/10.1128/AEM.02336-09>
- Bird, L. E., Ren, J., Zhang, J., Foxwell, N., Hawkins, A. R., Charles, I. G., & Stammers, D. K. (2002). Crystal structure of SANOS, a bacterial nitric oxide synthase oxygenase protein from *Staphylococcus aureus*. *Structure*, 10(12), 1687–1696.
- Bitan-Banin, G., Ortenberg, R., & Mevarech, M. (2003). Development of a gene knockout system for the halophilic archaeon *Haloferax volcanii* by use of the *pyrE* gene. *Journal of Bacteriology*, 185(3), 772–778. <https://doi.org/10.1128/jb.185.3.772-778.2003>
- Bogdan, C. (2015). Nitric oxide synthase in innate and adaptive immunity: an update. *Trends in Immunology*, 36(3), 161–178. <https://doi.org/10.1016/j.it.2015.01.003>
- Breuert, S., Allers, T., Spohn, G., & Soppa, J. (2006). Regulated polyploidy in halophilic archaea. *PLoS One*, 1, e92. <https://doi.org/10.1371/journal.pone.0000092>
- Chaudhari, S. S., Kim, M., Lei, S., Razvi, F., Alqarzaee, A. A., Hutflless, E. H., Powers, R., Zimmerman, M. C., Fey, P. D., & Thomas, V. C. (2017). Nitrite derived from endogenous bacterial nitric oxide synthase activity promotes aerobic respiration. *MBio*, 8(4), e00887-00817. <https://doi.org/10.1128/mBio.00887-17>
- Cinelli, M. A., Do, H. T., Miley, G. P., & Silverman, R. B. (2019). Inducible nitric oxide synthase: Regulation, structure, and inhibition. *Medicinal Research Reviews*, 40, 158–189. <https://doi.org/10.1002/med.21599>
- Costa, E. D., Rezende, B. A., Cortes, S. F., & Lemos, V. S. (2016). Neuronal nitric oxide synthase in vascular physiology and diseases. *Frontiers in Physiology*, 7, 206. <https://doi.org/10.3389/fphys.2016.00206>
- Crane, B. R., Sudhamsu, J., & Patel, B. A. (2010). Bacterial nitric oxide synthases. *Annual Review of Biochemistry*, 79, 445–470.
- Créach, V., Baudoux, A. C., Bertru, G., & Rouzic, B. L. (2003). Direct estimate of active bacteria: CTC use and limitations. *Journal of Microbiol Methods*, 52(1), 19–28.
- Czapski, G., & Goldstein, S. (1995). The role of the reactions of NO with superoxide and oxygen in biological systems: A kinetic approach. *Free Radical Biology and Medicine*, 19(6), 785–794.
- Derntl, C., Selb, R., Klein, R., Alte, B., & Witte, A. (2015). Genomic manipulations in alkaliphilic haloarchaea demonstrated by a gene disruption in *Natrialba magadii*. *FEMS Microbiology Letters*, 362(21), fnv179. <https://doi.org/10.1093/femsle/fnv179>
- Duetz, W. A., & Witholt, B. (2004). Oxygen transfer by orbital shaking of square vessels and deepwell microtiter plates of various dimensions. *Biochemical Engineering Journal*, 17(3), 181–185. [https://doi.org/10.1016/S1369-703X\(03\)00177-3](https://doi.org/10.1016/S1369-703X(03)00177-3)
- Ekiel, I., Sprott, G. D., & Smith, I. C. (1986). Mevalonic acid is partially synthesized from amino acids in *Halobacterium cutirubrum*: A ¹³C nuclear magnetic resonance study. *Journal of Bacteriology*, 166(2), 559–564.
- Falb, M., Müller, K., Königsmaier, L., Oberwinkler, T., Horn, P., von Gronau, S., Gonzalez, O., Pfeiffer, F., Bornberg-Bauer, E., & Oesterhelt, D. (2008). Metabolism of halophilic archaea. *Extremophiles*, 12(2), 177–196. <https://doi.org/10.1007/s00792-008-0138-x>
- Falb, M., Pfeiffer, F., Palm, P., Rodewald, K., Hickmann, V., Tittor, J., & Oesterhelt, D. (2005). Living with two extremes: conclusions from the genome sequence of *Natronomonas pharaonis*. *Genome Research*, 15(10), 1336–1343. <https://doi.org/10.1101/gr.3952905>
- Fischmann, T. O., Hruza, A., Niu, X. D., Fossetta, J. D., Lunn, C. A., Dolphin, E., Prongay, A. J., Reichert, P., Lundell, D. J., Narula, S. K., & Weber, P. C. (1999). Structural characterization of nitric oxide synthase isoforms reveals striking active-site conservation. *Nature Structural Biology*, 6, 233–242.
- Gillaspy, A. F., Hickmon, S. G., Skinner, R. A., Thomas, J. R., Nelson, C. L., & Smeltzer, M. S. (1995). Role of the accessory gene regulator (*agr*) in pathogenesis of staphylococcal osteomyelitis. *Infection and Immunity*, 63(9), 3373–3380.
- Gonzalez, O., Oberwinkler, T., Mansueto, L., Pfeiffer, F., Mendoza, E., Zimmer, R., & Oesterhelt, D. (2010). Characterization of growth and metabolism of the haloalkaliphile *Natronomonas pharaonis*. *PLoS Computational Biology*, 6(6), e1000799. <https://doi.org/10.1371/journal.pcbi.1000799>
- Gusarov, I., & Nudler, E. (2005). NO-mediated cytoprotection: Instant adaptation to oxidative stress in bacteria. *Proceedings of the National Academy of Sciences of the United States of America*, 102(39), 13855–13860. <https://doi.org/10.1073/pnas.0504307102>
- Gusarov, I., Shatalin, K., Starodubtseva, M., & Nudler, E. (2009). Endogenous nitric oxide protects bacteria against a wide spectrum of antibiotics. *Science*, 325(5946), 1380–1384. <https://doi.org/10.1126/science.1175439>
- Gusarov, I., Starodubtseva, M., Wang, Z. Q., McQuade, L., Lippard, S. J., Stuehr, D. J., & Nudler, E. (2008). Bacterial nitric-oxide synthases operate without a dedicated redox partner. *Journal of Biological Chemistry*, 283(19), 13140–13147. <https://doi.org/10.1074/jbc.M710178200>
- Haider, F. (2009). *Characterization of the DNA methyltransferase M.NmaphiCh11 and further characterization of a transformation system of haloalkaliphilic Archaea*. University of Vienna. Retrieved from https://urldefense.proofpoint.com/v2/url?u=http-3A__othes.univie.ac.at_5512_&d=DwlFaQ&c=sJ6xIWYx-zLMB3EPkvcnVg&r=P9m-u4034wbFAYPz5eKx4w&m=QANvoD_IY1ftsZ-26FnJ1o0tZrdOZKSC5WOzM2Xke9A&s=JFclIgd4AiLBse9XHj5yde1GRlcMY9guuTekcM7Ges&e
- Hanahan, D. (1983). Studies on transformation of *Escherichia coli* with plasmids. *Journal of Molecular Biology*, 166(4), 557–580. [https://doi.org/10.1016/s0022-2836\(83\)80284-8](https://doi.org/10.1016/s0022-2836(83)80284-8)
- Hanks, J. H., & Wallace, R. E. (1949). Relation of oxygen and temperature in the preservation of tissues by refrigeration. *Proceedings of the Society for Experimental Biology and Medicine*, 71(2), 196–200. <https://doi.org/10.3181/00379727-71-17131>
- Hansler, A., Chen, Q., Ma, Y., & Gross, S. S. (2016). Untargeted metabolite profiling reveals that nitric oxide bioynthesis is an endogenous modulator of carotenoid biosynthesis in *Deinococcus radiodurans* and is required for extreme ionizing radiation resistance. *Archives of Biochemistry and Biophysics*, 589, 38–52. <https://doi.org/10.1016/j.abb.2015.10.010>
- Humbard, M. A., Zhou, G., & Maupin-Furlow, J. A. (2009). The N-terminal penultimate residue of 20S proteasome alpha1 influences its N(alpha) acetylation and protein levels as well as growth rate and stress responses of *Haloferax volcanii*. *Journal of Bacteriology*, 191(12), 3794–3803. <https://doi.org/10.1128/JB.00090-09>
- James, K. L., Mogen, A. B., Brandwein, J. N., Orsini, S. S., Ridder, M. J., Markiewicz, M. A., Bose, J. L., & Rice, K. C. (2019). Interplay of nitric oxide synthase (NOS) and SrrAB in modulation of *Staphylococcus aureus* metabolism and virulence. *Infection and Immunity*, 87(2), <https://doi.org/10.1128/IAI.00570-18>
- Johnson, E. G., Sparks, J. P., Dzikovski, B., Crane, B. R., Gibson, D. M., & Loria, R. (2008). Plant-pathogenic *Streptomyces* species produce nitric oxide synthase-derived nitric oxide in response to host signals. *Chemistry & Biology*, 15(1), 43–50. <https://doi.org/10.1016/j.chembiol.2007.11.014>
- Jones, D. L., & Baxter, B. K. (2017). DNA repair and photoprotection: Mechanisms of overcoming environmental ultraviolet radiation exposure in halophilic archaea. *Frontiers in Microbiology*, 8, 1882. <https://doi.org/10.3389/fmicb.2017.01882>

- Jourd'heuil, D., Kang, D., & Grisham, M. B. (1997). Interactions between superoxide and nitric oxide: Implications in DNA damage and mutagenesis. *Frontiers in Bioscience*, 2, d189–d196.
- Kinkel, T. L., Ramos-Montañez, S., Pando, J. M., Tadeo, D. V., Strom, E. N., Libby, S. J., & Fang, F. C. (2016). An essential role for bacterial nitric oxide synthase in *Staphylococcus aureus* electron transfer and colonization. *Nat Microbiol*, 2, 16224. <https://doi.org/10.1038/nmicriobiol.2016.224>
- Knowles, R. G., & Moncada, S. (1994). Nitric oxide synthases in mammals. *The Biochemical Journal*, 298(Pt 2), 249–258.
- Lancaster, J. R. (1994). Simulation of the diffusion and reaction of endogenously produced nitric oxide. *Proceedings of the National Academy of Sciences of the United States of America*, 91(17), 8137–8141.
- Lazrak, T., Wolff, G., Albrecht, A.-M., Nakatani, Y., Ourisson, G., & Kates, M. (1988). Bacterioruberins reinforce reconstituted *Halobacterium* lipid membranes. *Biochimica Et Biophysica Acta (BBA) - Biomembranes*, 939(1), 160–162.
- Lewis, A. M., Matzdorf, S. S., Endres, J. L., Windham, I. H., Bayles, K. W., & Rice, K. C. (2015). Examination of the *Staphylococcus aureus* nitric oxide reductase (saNOR) reveals its contribution to modulating intracellular NO levels and cellular respiration. *Molecular Microbiology*, 96(3), 651–669. <https://doi.org/10.1111/mmi.12962>
- Lewis, A. M., Matzdorf, S. S., & Rice, K. C. (2016). Fluorescent detection of intracellular nitric oxide in *Staphylococcus aureus*. *Bio-protocol*, 6(14), e1878. <https://doi.org/10.21769/BioProtoc.1878>
- Liu, H., Han, J., Liu, X., Zhou, J., & Xiang, H. (2011). Development of *pyrF*-based gene knockout systems for genome-wide manipulation of the archaea *Haloferax mediterranei* and *Haloarcula hispanica*. *Journal of Genetics and Genomics*, 38(6), 261–269. <https://doi.org/10.1016/j.jgg.2011.05.003>
- Mashruwala, A. A., Roberts, C. A., Bhatt, S., May, K. L., Carroll, R. K., Shaw, L. N., & Boyd, J. M. (2016). *Staphylococcus aureus* SufT: an essential iron-sulphur cluster assembly factor in cells experiencing a high-demand for lipoic acid. *Molecular Microbiology*, 102, 1099–1119.
- Mayrhofer-Iro, M., Ladurner, A., Meissner, C., Derntl, C., Reiter, M., Haider, F., Dimmel, K., Rössler, N., Klein, R., Baranyi, U., Scholz, H., & Witte, A. (2013). Utilization of virus ϕ Ch1 elements to establish a shuttle vector system for Halo(alkali)philic Archaea via transformation of *Natrialba magadii*. *Applied and Environmental Microbiology*, 79(8), 2741–2748. <https://doi.org/10.1128/AEM.03287-12>
- Miller, N. J., Sampson, J., Candeias, L. P., Bramley, P. M., & Rice-Evans, C. A. (1996). Antioxidant activities of carotenes and xanthophylls. *FEBS Letters*, 384(3), 240–242.
- Mogen, A. B., Carroll, R. K., James, K. L., Lima, G., Silva, D., Culver, J. A., Petucci, C., Shaw, L. N., & Rice, K. C. (2017). *Staphylococcus aureus* nitric oxide synthase (saNOS) modulates aerobic respiratory metabolism and cell physiology. *Molecular Microbiology*, 105(1), 139–157. <https://doi.org/10.1111/mmi.13693>
- Montgomery, H. J., Dupont, A. L., Leivo, H. E., & Guillemette, J. G. (2010). Cloning, expression, and purification of a nitric oxide synthase-like protein from *Bacillus cereus*. *Biochemistry Research International*, 2010, 489892. <https://doi.org/10.1155/2010/489892>
- Norrander, J., Kempe, T., & Messing, J. (1983). Construction of improved M13 vectors using oligodeoxynucleotide-directed mutagenesis. *Gene*, 26(1), 101–106. [https://doi.org/10.1016/0378-1119\(83\)90040-9](https://doi.org/10.1016/0378-1119(83)90040-9)
- Pant, K., Bilwes, A. M., Adak, S., Stuehr, D. J., & Crane, B. R. (2002). Structure of a nitric oxide synthase heme protein from *Bacillus subtilis*. *Biochemistry*, 41(37), 11071–11079.
- Patel, B. A., Moreau, M., Widom, J., Chen, H., Yin, L., Hua, Y., & Crane, B. R. (2009). Endogenous nitric oxide regulates the recovery of the radiation-resistant bacterium *Deinococcus radiodurans* from exposure to UV light. *Proceedings of the National Academy of Sciences of the United States of America*, 106(43), 18183–18188. <https://doi.org/10.1073/pnas.0907262106>
- Popova, T. G., Teunis, A., Vaseghi, H., Zhou, W., Espina, V., Liotta, L. A., & Popov, S. G. (2015). Nitric oxide as a regulator of *B. anthracis* pathogenicity. *Frontiers in Microbiology*, 6, 921. <https://doi.org/10.3389/fmicb.2015.00921>
- Pufahl, R. A., Wishnok, J. S., & Marletta, M. A. (1995). Hydrogen peroxide-supported oxidation of NG-hydroxy-L-arginine by nitric oxide synthase. *Biochemistry*, 34(6), 1930–1941.
- Ras, G., Zuliani, V., Derkx, P., Seibert, T. M., Leroy, S., & Talon, R. (2017). Evidence for nitric oxide synthase activity in *Staphylococcus xylosus* mediating nitrosoheme formation. *Frontiers in Microbiology*, 8, 598. <https://doi.org/10.3389/fmicb.2017.00598>
- Reece, S. Y., Woodward, J. J., & Marletta, M. A. (2009). Synthesis of nitric oxide by the NOS-like protein from *Deinococcus radiodurans*: a direct role for tetrahydrofolate. *Biochemistry*, 48(23), 5483–5491. <https://doi.org/10.1021/bi900385g>
- Rodrigo-Baños, M., Garbayo, I., Vilchez, C., Bonete, M. J., & Martínez-Espinosa, R. M. (2015). Carotenoids from haloarchaea and their potential in biotechnology. *Mar Drugs*, 13(9), 5508–5532. <https://doi.org/10.3390/md13095508>
- Sapp, A. M., Mogen, A. B., Almand, E. A., Rivera, F. E., Shaw, L. N., Richardson, A. R., & Rice, K. C. (2014). Contribution of the *nospdt* operon to virulence phenotypes in methicillin-sensitive *Staphylococcus aureus*. *PLoS One*, 9(9), e108868. <https://doi.org/10.1371/journal.pone.0108868>
- Sasaki, T., Razak, N. W., Kato, N., & Mukai, Y. (2012). Characteristics of halorhodopsin-bacterioruberin complex from *Natronomonas pharaonis* membrane in the solubilized system. *Biochemistry*, 51(13), 2785–2794. <https://doi.org/10.1021/bi201876p>
- Sievers, F., Wilm, A., Dineen, D., Gibson, T. J., Karplus, K., Li, W., Lopez, R., McWilliam, H., Remmert, M., Söding, J., Thompson, J. D., & Higgins, D. G. (2011). Fast, scalable generation of high-quality protein multiple sequence alignments using Clustal Omega. *Molecular Systems Biology*, 7, 539. <https://doi.org/10.1038/msb.2011.75>
- Smith, J. J., & McFeters, G. A. (1996). Effects of substrates and phosphate on INT (2-(4-iodophenyl)-3-(4-nitrophenyl)-5-phenyl tetrazolium chloride) and CTC (5-cyano-2,3-ditolyl tetrazolium chloride) reduction in *Escherichia coli*. *Journal of Applied Bacteriology*, 80(2), 209–215.
- Stachler, A. E., & Marchfelder, A. (2016). Gene repression in haloarchaea using the CRISPR (Clustered Regularly Interspaced Short Palindromic Repeats)-Cas I-B system. *Journal of Biological Chemistry*, 291(29), 15226–15242. <https://doi.org/10.1074/jbc.M116.724062>
- Stuehr, D. J., Santolini, J., Wang, Z. Q., Wei, C. C., & Adak, S. (2004). Update on mechanism and catalytic regulation in the NO synthases. *Journal of Biological Chemistry*, 279(35), 36167–36170. <https://doi.org/10.1074/jbc.R400017200>
- Sudhamsu, J., & Crane, B. R. (2009). Bacterial nitric oxide synthases: What are they good for? *Trends in Microbiology*, 17(5), 212–218. <https://doi.org/10.1016/j.tim.2009.02.003>
- van Sorge, N. M., Beasley, F. C., Gusarov, I., Gonzalez, D. J., von Köckritz-Blickwede, M., Anik, S., Borkowski, A. W., Dorrestein, P. C., Nudler, E., & Nizet, V. (2013). Methicillin-resistant *Staphylococcus aureus* bacterial nitric-oxide synthase affects antibiotic sensitivity and skin abscess development. *Journal of Biological Chemistry*, 288(9), 6417–6426. <https://doi.org/10.1074/jbc.M112.448738>
- Wang, Z. Q., Lawson, R. J., Buddha, M. R., Wei, C. C., Crane, B. R., Munro, A. W., & Stuehr, D. J. (2007). Bacterial flavodoxins support nitric oxide production by *Bacillus subtilis* nitric-oxide synthase. *Journal of Biological Chemistry*, 282(4), 2196–2202. <https://doi.org/10.1074/jbc.M608206200>
- Wang, Z. Q., Wei, C. C., Sharma, M., Pant, K., Crane, B. R., & Stuehr, D. J. (2004). A conserved Val to Ile switch near the heme pocket of animal and bacterial nitric-oxide synthases helps determine their

- distinct catalytic profiles. *Journal of Biological Chemistry*, 279(18), 19018–19025. <https://doi.org/10.1074/jbc.M311663200>
- Weisslocker-Schaetzel, M., Lembrouk, M., Santolini, J., & Dorlet, P. (2017). Revisiting the Val/Ile mutation in mammalian and bacterial nitric oxide synthases: A spectroscopic and kinetic study. *Biochemistry*, 56(5), 748–756. <https://doi.org/10.1021/acs.biochem.6b01018>
- Wink, D. A., Grisham, M. B., Mitchell, J. B., & Ford, P. C. (1996). Direct and indirect effects of nitric oxide in chemical reactions relevant to biology. *Methods in Enzymology*, 268, 12–31.
- Yanisch-Perron, C., Vieira, J., & Messing, J. (1985). Improved M13 phage cloning vectors and host strains: Nucleotide sequences of the M13mp18 and pUC19 vectors. *Gene*, 33(1), 103–119. [https://doi.org/10.1016/0378-1119\(85\)90120-9](https://doi.org/10.1016/0378-1119(85)90120-9)

- Zhou, L., & Zhu, D. Y. (2009). Neuronal nitric oxide synthase: structure, subcellular localization, regulation, and clinical implications. *Nitric Oxide*, 20(4), 223–230. <https://doi.org/10.1016/j.niox.2009.03.001>

How to cite this article: Orsini SS, James KL, Reyes DJ, et al. Bacterial-like nitric oxide synthase in the haloalkaliphilic archaeon *Natronomonas pharaonis*. *MicrobiologyOpen*. 2020;9:e1124. <https://doi.org/10.1002/mbo3.1124>

APPENDIX

ADDITIONAL METHODS

Recipes for modified DSM 205 and NVM+ media used in this study:

Modified DSM 205	
Casamino acids	15 g
Tri-Na citrate	3.0 g
Glutamic acid	2.5 g
MgSO ₄ × 7H ₂ O	2.5 g
KCl	2.0 g
NaCl	204 g
H ₂ O	950 ml

Autoclave, then add 12 ml of filter-sterilized 20% Na₂CO₃ to adjust pH to 8.5.

NVM+	
Casamino acids	8.8 g
Yeast extract	11.7 g
Tri-Na citrate	0.8 g
KCl	2.35 g
NaCl	235 g
H ₂ O up to for plates	934 ml
Agar	8 g

After autoclaving, the medium or the agar was completed with:

0.57 M Na ₂ CO ₃ filter sterilized	65 ml
1 M MgSO ₄ (autoclaved)	1 ml
20 mM FeSO ₄ filter sterilized	1 ml
20% Na ₂ CO ₃ filter sterilized	Until pH reaches 9.0

Bioinformatics analysis

The *S. aureus* MRSA252 *nos* open reading frame (GenPept accession# CAG40992) was used to tBLASTn search (Altschul et al., 1990) the NCBI RefSeq genome database, restricting the search to Archaea (TAXID 2157). Clustal Omega (Sievers et al., 2011) was used to align the saNOS AA sequence from *S. aureus* MRSA 252 (CAG40992) to NOS AA sequences in the following organisms (GenPept accession #s indicated in brackets): *B. subtilis* 168 (AQR84931.1), *Nmn. pharaonis* DSM 2160 (CAI49045.1), *Natronobacterium gregoryi* SP2 (AFZ73990.1), *Natronolimnobius aegyptiacus* (ARS90434.1), *Halorientalis* sp. IM1011 (AQL41467.1), *Halobiforma nitratireducens* JCM 10879 (EMA47161.1), *Halostagnicola kamekurae* (SFS56640.1), *Haloplanus salinus* (RCU47147.1), *Halalkalicoccus paucihalophilus* (KYH24998.1), *Halonotius pteroides* (RJX51750.1), *Halovenus aranensis* (SDK10415.1).

DNA isolation and genome re-sequencing

Mid-exponential phase aerobically grown cultures of wild type and *nos* mutant A2 were harvested by centrifugation and genomic DNA was isolated from each strain using Qiagen Genomic-tip 100/G columns and manufacturers protocols for bacterial DNA isolation. Genomic DNA was submitted to the UF-ICBR NextGen DNA sequencing for barcoding, library construction, and subsequent Illumina MiSeq sequencing (2x300 cycles, paired-end format) with v3 Illumina sequencing reagents. Whole-genome sequencing data was analyzed using the CLC Genomics Workbench software package (Qiagen) as previously described (Mashruwala et al., 2016). In brief, sequencing reads were aligned to the *Nmn. pharaonis* DSM 2160 reference genome (NC_007426.1). Quality-based variant detection was performed to identify polymorphisms in each sequenced strain. SNPs with a minimum 40% frequency of detection were reported in this study.

Strain or plasmid	Description	Source or references
<i>E. coli</i> DH5 α	dlacZ Delta M15 Delta(lacZYA-argF) U169 recA1 endA1 hsdR17(rK-mK+) supE44 thi-1 gyrA96	Hanahan (1983)
<i>E. coli</i> JM110	<i>rpsL (Strr) thr leu thi-1 lacY galK galT ara tonA tsx dam dcm supE44 Δ(lac-proAB)</i>	Yanisch-Perron et al. (1985)
<i>E. coli</i> BL21(DE3)	<i>F- ompT hsdSB (rBmB-) gal dcm (DE3)</i>	Novagen
<i>Nmn. pharaonis</i>	Wild-type DSM 2160	ATCC 35678
<i>Nmn. pharaonis</i> A2	<i>nos::gyrB</i> mutation	This publication
<i>Hfx. volcanii</i> H26	Δ <i>pyrE2</i> derivative of <i>Hfx. volcanii</i> D70	Allers et al. (2004)
pUC19	<i>bla</i> (AmpR)	Norrander et al. (1983)
pCRBlunt	KanR, MCS	Invitrogen
pUC19-npnos	NP-1908A (<i>nos</i>) cloned into pUC19 at EcoRI and HindIII sites	This publication
pJAM809	Source of <i>gyrB</i> gene	Humbard et al. (2009)
pUC19nos:: <i>gyrB</i>	<i>bla</i> (AmpR), <i>gyrB</i> (NovR), <i>Nmn. pharaonis nos</i> disrupted	This publication
pET24b	N-terminal T7•Tag, C-terminal His•Tag, KanR	Novagen
pET24b-npNOS	<i>Natronomonas pharaonis nos</i> with C-terminal His•Tag, KanR	This publication
pET24b-saNOS	<i>Staphylococcus aureus nos</i> with C-terminal His•Tag, KanR	This publication
pRO5	ϕ Ch1 and ColE1 origins of replication; <i>bla</i> (AmpR), <i>gyrB</i> (NovR)	Mayrhofer-Iro et al. (2013)

TABLE A1 Bacterial and archaeal strains and plasmids used in this study

TABLE A2 Primers used in this study

Primer	Sequence (5'–3')
Npnos_NdeI_F	CATATGCACGAGCCGCGAG
Npnos_NotI_R	TGCGGCCGCGAGCGATTCCCGCCGCTC
Sanos_NdeI_F	CATATGTATTAAAGAGGCTCAAGC
Sanos_XhoI_R	CTCGAGCCAGTGCCCTTCCATCAT
Npnos_EcoRI_F	AGTGAATTCATGCACGAGCCGCGCGAG
Npnos_HindIII_R	GCCAAGCTTTCAGCGCCGAGCGA
Npnos_promoter_F	GTTTAATGGTTACGAAGTGCCCA
Npnos_check_R	TCAGCGCCGAGCGATTCC
<i>gyrB</i> _check_R	TCTCACCGAGTCCCTTGAAC

TABLE A3 Archaeal NOS homologs identified by tBLASTn search using the saNOS amino acid sequence from MRSA252 (CAG40992)

Description	Query cover	Order	E-value	%Identity	Genome accession
<i>Natronobacterium gregoryi</i> SP2, complete genome	96%	Natrialbales	3.00E ⁻¹¹⁴	50.99%	NC_019792.1
<i>Halobiforma nitratireducens</i> JCM 10879 contig_3, whole-genome shotgun sequence	96%	Natrialbales	2.00E ⁻¹¹⁰	49.44%	NZ_AOMA01000003.1
<i>Natronobacterium texcoconense</i> strain DSM 24767, whole-genome shotgun sequence	96%	Natrialbales	5.00E ⁻¹¹⁰	50.00%	NZ_FNLCO1000002.1
<i>Natronolimnobius</i> sp. AArc1 chromosome, complete genome	95%	Natrialbales	3.00E ⁻¹⁰⁶	48.72%	NZ_CP024047.1
<i>Natronomonas</i> sp. F20-122 NODE_2_length_675769_cov_15.592506, whole-genome shotgun sequence	96%	Halobacteriales	7.00E ⁻¹⁰⁶	49.86%	NZ_QKNX01000002.1
<i>Natronolimnobius</i> sp. AArc-Mg chromosome, complete genome	95%	Natrialbales	9.00E ⁻¹⁰⁶	48.72%	NZ_CP027033.1
<i>Natronolimnobius aegyptiacus</i> strain JW/ NM-HA 15 chromosome, complete genome	98%	Natrialbales	4.00E ⁻¹⁰⁴	45.00%	NZ_CP019893.1
<i>Halostagnicola kamekurae</i> strain DSM 22427, whole-genome shotgun sequence	96%	Natrialbales	2.00E ⁻¹⁰³	48.58%	NZ_FOZS01000001.1
<i>Natronomonas pharaonis</i> DSM 2160 complete genome	95%	Halobacteriales	3.00E ⁻¹⁰³	48.43%	NC_007426.1
<i>Halostagnicola</i> sp. A56 14, whole-genome shotgun sequence	96%	Natrialbales	6.00E ⁻¹⁰³	48.30%	NZ_JMIP02000014.1
<i>Halorientalis</i> sp. IM1011, complete genome	98%	Halobacteriales	2.00E ⁻¹⁰¹	46.67%	NZ_CP019067.1
<i>Haloplanus salinus</i> strain JCM 18368 contig00001, whole-genome shotgun sequence	96%	Haloferacales	7.00E ⁻¹⁰¹	47.32%	NZ_QPHM01000001.1
<i>Halalkalicoccus paucihalophilus</i> strain DSM 24557 HAPAU_contig000010, whole-genome shotgun sequence	98%	Halobacteriales	8.00E ⁻¹⁰¹	46.67%	NZ_LTAZ01000010.1
<i>Halonotius pteroides</i> strain CECT 7525 NODE_1_length_283971_cov_232.584, whole-genome shotgun sequence	94%	Haloferacales	3.00E ⁻¹⁰⁰	48.99%	NZ_QMDW01000001.1
<i>Halovenus aranensis</i> strain IBRC-M10015, whole-genome shotgun sequence	96%	Halobacteriales	4.00E ⁻⁹⁶	44.89%	NZ_FNFC01000018.1

Open Access

<i>S. aureus</i>	-----MLFKEAQAFIENMYKECHYETQI INKRLHDIELEIKETGTYTHTTEBELI	49
<i>B. subtilis</i>	-----MEEKEI LWNKAFIAACYQELGKEEE-VKDRDLADIKSEIDL TGSYVHTKEELE	53
<i>Halovenus</i>	MHSASTYGRDRYEAENFLRQCYKELGREGD-VESRLKEVWTSIGRQNHVHTTAELE	59
<i>Haloplanus</i>	MNVDPQEYGRMERYEAAEAFVRCYEEELGRESE-IDDRLELWTSIGRRDHVHTTAELE	59
<i>Halonotius</i>	-----MSKQERHEAADFDIEQCYAECREDDD-VDERLEAIWHAIGRTGHVHTTSMLE	52
<i>Natronobacterium</i>	MHAPVPEHDPEDLYAEAEAFVRCYAELENEDE-IEPRLAERASIAESGHYEHTPEELE	59
<i>Halobiforma</i>	MHAPVPEYEPTELYAEAEAFVRCYSELGRDDE-IDDRLETVRRSIAESGHYEHTPAELE	59
<i>Natronolimnobius</i>	MHQPIPEYDPQELYREAEAFVRCYTELEKESA-IEPRLETIRREIAESGHYDHTPEELE	59
<i>Natronomonas</i>	MHEPPQEYSREERFAEAKSFIQCYTELGRESE-IDDRLEAEIAEIERRNHYEHTPEELE	59
<i>Halalkalicoccus</i>	MPGSFFEYSQELYEAADAFIRDCYAEELGRESE-IDDRLEDAEIAEIQRGHYDHTSPELE	59
<i>Halorientalis</i>	MHESPEYSRRELYEAADAFVRCYSELGRESE-IDDRLEDAEIEERRGHYDHTTAELE	59
<i>Halostagnicola</i>	MHASPTSEYSPRELYEAADAFVRCYSELGRESE-IDDRLEDAEIEERRGRYEHTSPELE	59
	* * * * * : : * * * * * : * * * * *	
<i>S. aureus</i>	YGAKMARNSNRIGR LF WDSLNVIDARDVTDEASFLSSINHYIAQATNEGKIKYITIT	109
<i>B. subtilis</i>	HGAKMARNSNRIGR LF WNSLNVIDRRDVRTKEEVRDALFHHEIETATNNGKIRITITIF	113
<i>Halovenus</i>	HGAKMARNSNRIGR LF WDSLHLVDRRGIDTAQGVYALIEHIDFATNDGNIRITISVF	119
<i>Haloplanus</i>	RGAKMARNSNRIGR LF WDRHLVLDRRDVTAAAVFDALLDHVEFATNGGNVIRITISVF	119
<i>Halonotius</i>	HGAKMARNSNRIGR LF WDSLVRDCEATTAEEAYDELVSHITTTATNDGNIVITISVF	112
<i>Natronobacterium</i>	HGARMARNSNRIGR LF WETLVDVIDARDADDAESYDALCHHLEYATNDGDIRITITVF	119
<i>Halobiforma</i>	YGAKLARNSNRIGR LF WETLVDVIDARDRTAEVYDALCGHLEQATNGGDIRITITVF	119
<i>Natronolimnobius</i>	HGARMARNSNRIGR LF WQSLVLDRRDCEATPAEVHEACCEHLDRARNGGDIRITISVF	119
<i>Natronomonas</i>	HGAKMARNSNRIGR LF WQQLNVADDERDCEATAEVHEACCRHLEKARNGGDIRITISVF	119
<i>Halalkalicoccus</i>	HGAKMARNSNRIGR LF WHHLNVADARDCETAREVHEACCTHLERARNGGDIRITISVF	119
<i>Halorientalis</i>	HGAKMARNSNRIGR LF WQQLTVADARDCETAREVHEACCTHLERARNGGDIRITISVF	119
<i>Halostagnicola</i>	HGAKMARNSNRIGR LF WQQLNVADARDCETAREVHEACCRHLERARNGGDIRITISVF	119
	* * * * * : : * * * * * : * * * * *	
<i>S. aureus</i>	APKD----GPKIFNNQLIRYAGYDNC-----GDPAEKEVTRLA	143
<i>B. subtilis</i>	PPEEKGEKQVEIWNHQLIRYAGYESD-----GERIGDPASCSLTAAC	155
<i>Halovenus</i>	PPAVRGNQVRIWNHQLIRYAGYETE-----NGVIGDPNSVALTDYC	161
<i>Haloplanus</i>	PPAVRGEQVRIWNHQLIRYAGYRTD-----DGVVGDPPDSTALTDYC	161
<i>Halonotius</i>	PPAAVQENPRVRIWNHQLIRYAGYETD-----SGVVGDPPDSTALTDYC	154
<i>Natronobacterium</i>	EPMVRGKQVQIWNHQLIRYAGYETD-----DGIVGDPAEVEFTTEYC	161
<i>Halobiforma</i>	EPMIRGRQVRLWNHQLIRYAGYETD-----DGIVGDPAEVEFTTEYC	161
<i>Natronolimnobius</i>	EPMIRGRQVRIWNHQLIRYAGYAGDDSDVVTGGDRTRAENPDEIVGDPAEVPMTRYC	179
<i>Natronomonas</i>	KPMVDGDRQVRIWNHQLIRYAGYRTD-----DGIVGDPAEVEFTTEYC	161
<i>Halalkalicoccus</i>	KPIIKGEQVRLWNHQLIRYAGYQTE-----DGIVGDPAEVEFTTEYC	161
<i>Halorientalis</i>	KPMIDGDRQVRLWNHQLIRYAGYRTA-----DGIVGDPAEVEFTTEYC	161
<i>Halostagnicola</i>	KPMIDGHEQVRLWNHQLIRYAGYRTE-----DGVVGDPAEVEFTTEYC	161
	: : * * * * * : : * * * * * : * * * * *	
<i>S. aureus</i>	NHLGWKGGKTNFDVPLVIQYL-PNESVKYIEYPTSLIKEVPIEHDHYPKLRKLNWKYAV	202
<i>B. subtilis</i>	EELGWRGERTDFDPLPIFRMKGDEQPWYELPRSLVIEVPIHTHPIEAFSDLELKWYGV	215
<i>Halovenus</i>	RSRGWSSQRTDFDPLPIQV-GDKTPELFEIPDDVMEVPLSHPNYQWFSDLGLQWYAV	220
<i>Haloplanus</i>	RDRGWSGAGTEFDVPLPIQV-GDDEPELFEIPDELVLVLEPLVHPEYDFEALALQWYAV	220
<i>Halonotius</i>	QSRGWSGEGTFDPLPIQI-GDREPELFEIPDELVLVLEPLVHPEYDFEALGLQWYAV	213
<i>Natronobacterium</i>	QSRGWEGDETDVPLVQVQ-LRNEPELFEVPPDLELVEPIHHPDHDWIADLDLQWYAV	220
<i>Halobiforma</i>	QSRGWESSETEFDVLPVQVQ-EDREPELFEVPPDLELVEPIHPEYDFEALGLQWYAV	220
<i>Natronolimnobius</i>	QSRGWEGDGRFDILPHVIQV-GDDEPELFEVPPDSVIEEVELSHPEYDFEALDLRWYDV	238
<i>Natronomonas</i>	QSRGWEGDGTDFDILPHVIQV-GDDEPELFEVPPDSAVGVEPLRHPDYEFEDLGLRWYDV	220
<i>Halalkalicoccus</i>	QSRGWEGEGTRFDILPHVIQI-QDQPELFEVPPESAI GEVRLRHPDYEFEDLGLRWYDV	220
<i>Halorientalis</i>	QSRGWEGEGTRFDILPHVQI-RDQPELFEVPPESAVGEVRLRHPDYEFEDLGLRWYDV	220
<i>Halostagnicola</i>	QSRGWEGEGTRFDILPHVIQI-RDQPELFEVPPESVVEVRLRHPDYEFEDLGLRWYDV	220
	: : * * * * * : : * * * * * : * * * * *	
<i>S. aureus</i>	PIISNMDLKIIGGIVYPTAPNGY Y VTIGV RNF IDDYRYNLEKVADEFEDTLK NSF	262
<i>B. subtilis</i>	PIISDMKLEVGGIHYNAAPNGY Y YGTIGARNLADEKRYDKLKKVASVIGIAADYDNTDL	275
<i>Halovenus</i>	PIISDMRLEIGGLQYPAAPNGY Y YGTIGSRNFGVDVRYDMLPTVADQLGLDTSRDL	280
<i>Haloplanus</i>	PIISDMRLEIGRIRYPAAPNGY Y YGTIGSRDLGDTDRYDVLPRADRLGLTTTDRSL	280
<i>Halonotius</i>	PIISDMRLEIGGLQYPAAPNGY Y YGTIGSRDLGDTDRYDMLPEVATRLGLDTRDRSL	273
<i>Natronobacterium</i>	PVVSNMRLIEIGGLQYTAAPNGY Y YATIAARNFADEDYDMLPAVAERLGLDTRNRDL	280
<i>Halobiforma</i>	PVVSNMRLIEIGGLQYTAAPNGY Y YATIAARNFADEDYDMLPAVAERLGLDTRNRDL	280
<i>Natronolimnobius</i>	PVVSNMRLIEIGGLQYTAAPNGY Y YATIGARNFADTDYDMLPEIADRLGLDTRDRSL	298
<i>Natronomonas</i>	PVVSNMRLIEIGGLQYTAAPNGY Y YATIGARNLADEDYDMLPTVAERLGLDTRDRSL	280
<i>Halalkalicoccus</i>	PVVSNMRLIEIGGLQYTAAPNGY Y YATIGARNLADEDYDMLPTVAERLGLDTRDRSL	280
<i>Halorientalis</i>	PVVSNMRLIEIGGLQYTAAPNGY Y YATIGARNLADEDYDMLPAVAERLGLDTRDRSL	280
<i>Halostagnicola</i>	PVVSNMRLIEIGGLQYTAAPNGY Y YATIGARNLADEDYDMLPAVAERLGLDTRDRSL	280
	* * * * * : : * * * * * : * * * * *	
<i>S. aureus</i>	NKDRALVELNVAVYHSFKKEGVSIVDHLTAAKQFELFERNEAQGRQVTKGWSWLLAPLS	322
<i>B. subtilis</i>	WKDQALVELNKAHLVHSYKQGVIVDHHHTAASQFARFEEQEEAAGRKLTDGWTWLIPTIS	335
<i>Halovenus</i>	WKDEALVALNQAHLVHSYKQGVIVDHHHTAASQFARFEEQEEAAGRKVTGERSWLLPPNA	340
<i>Haloplanus</i>	WKDRALTVLNRVHLVHSYKQGVIVDHHHTAASQFARFEEQEEAAGRVTGDRSWLLPPNA	340
<i>Halonotius</i>	WKDQALTVLNRVHLVHSYKQGVIVDHHHTAASQFARFEEQEEAAGRVTGDRSWLLPPNA	333
<i>Natronobacterium</i>	WKDEALVELNRAHLVHSYDRTGVRIVDHHHTAASQFARFEEQEEAAGRVTGDRSWLLPPVS	340
<i>Halobiforma</i>	WKDEALVALNRAHLVHSYDRTGVRIVDHHHTAASQFARFEEQEEAAGRVTGDRSWLLPPMS	340
<i>Natronolimnobius</i>	WKDEALVELNRAHLVHSYDRTGVRIVDHHHTVTDQFARFEEQEEAAGRVTGDRSWLLPPVS	358
<i>Natronomonas</i>	WKDEALVELNRAHLVHSYDRTGVRIVDHHHTVTDQFARFEEQEEAAGRVTGDRSWLLPPMS	340
<i>Halalkalicoccus</i>	WKDEALVALNRAHLVHSYDRTGVRIVDHHHTVTDQFARFEEQEEAAGRVTGERSWLLPPMS	340
<i>Halorientalis</i>	WKDEALVELNRAHLVHSYDRTGVRIVDHHHTVTDQFARFEEQEEAAGRVTGDRSWLLPPMS	340
<i>Halostagnicola</i>	WKDEALVELNRAHLVHSYDRTGVRIVDHHHTVTDQFARFEEQEEAAGRVTGDRSWLLPPMS	340
	* * * * * : : * * * * * : * * * * *	
<i>S. aureus</i>	PTLTSNYH HYDNTVKDPNEFYK KK SNANQCPFH--	358
<i>B. subtilis</i>	PAATHIFHRSDNSIVKPNFYQDKPYE-----	363
<i>Halovenus</i>	SSTVHIFHENTYENEIRTPNEYREDPPPLQ-----	370
<i>Haloplanus</i>	SSTHIFHFDYDDVVRTPNNEYRDEPAPLR-----	370
<i>Halonotius</i>	SSTVHIFDEEYDVTVRTPNNEYRDDPLTM-----	362
<i>Natronobacterium</i>	PASTHIFHKKYENRVETPNNEYREPPYEDCSDDSS---	375
<i>Halobiforma</i>	SATTHVFHNEYDVTVKTPNEYRESPEYKDTGT-----	373
<i>Natronolimnobius</i>	PATTVQVHHTYDDEIRTPNEYLEPPAIRE-----	389
<i>Natronomonas</i>	SATTHVFSNDYDRIEKPNEYQAPEPLSERRESLGR	378
<i>Halalkalicoccus</i>	SATTHVFENDYDNTIKKPNNEYQAPEPLSERRESLSR	378
<i>Halorientalis</i>	SATTHVFENDYDNTIKKPNNEYQAPEPLSERRESLGR	378
<i>Halostagnicola</i>	PATTHVFENDYDNTVEKPNNEYQDPPAGLTERRESLGR	378
	: : * * * * * : : * * * * *	

Figure A1 CLUSTAL O (1.2.4) multiple sequence alignment of representative archaeal NOS homologs with *S. aureus* and *B. subtilis* NOS. Blue = conserved dimerization residue in bacterial NOS; black underline = dimerization regions (saNOS); green = heme-binding residues (saNOS); Red = active-site residues (saNOS); orange = predicted bacterial NOS interaction site with reductase domain (line the pocket where heme edge is exposed); conserved sequence (*), conservative mutations (:), semi-conservative mutations (.), and non-conservative mutations (). Conserved residues denoted in color above have been reported in (Alderton et al., 2001; Bird et al., 2002; Crane et al., 2010; Fischmann et al., 1999)

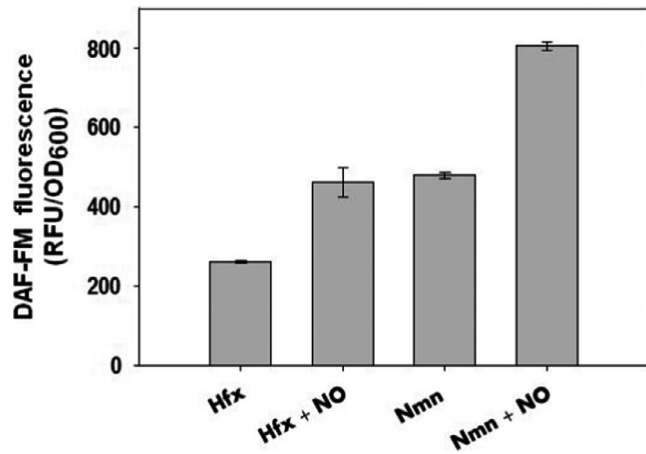


Figure A2 Intracellular NO/RNS detection by DAF-FM diacetate. *Hfx. volcanii* and *Nmn. pharaonis* early exponential-phase cells were stained with 5 μ M DAF-FM diacetate as described in Section 2. Cells were then incubated in buffer alone or buffer containing 100 μ M diethylamine-NONOate donor. DAF-FM fluorescence was measured after 45 min using a Biotek Synergy microplate reader. DAF-FM fluorescence reported as relative fluorescent units (RFU) per OD of each sample. Data representative of $n = 3$ independent experiments, error bars = SEM

TABLE A4 SNP analysis of re-sequenced wild type and *nos::gyrB* mutant to published *Nmn. pharaonis* DSM 2160 reference genome (NC_007426.1).

Reference Position	Type	Length	Reference	Allele	Count	Coverage	Frequency	Forward/reverse balance	Average quality	Protein Description	Locus Tag	Coding region change	Amino acid change
1061	SNV	1	G	A	494	499	99	0.48	34.22	Predicted restriction endonuclease	NP_000_2A	WP_011321731.1:c.46C>T	WP_011321731.1:p.Pro16Ser
177659	SNV	1	C	G	542	545	99.45	0.49	34.72	hypothetical protein	NP_033_8A	WP_011321898.1:c.278G>C	WP_011321898.1:p.Gly93Ala
501766	SNV	1	C	T	471	472	99.79	0.48	34.64	F0F1 ATP synthase subunit C	NP_102_2A	WP_011322237.1:c.227C>T	WP_011322237.1:p.Ala76Val
504445	SNV	1	G	A	511	511	100	0.5	34.67	ATP synthase subunit A	NP_103_0A	WP_011322241.1:c.649G>A	WP_011322241.1:p.Gly217Ser
1017698	SNV	1	G	T	444	445	99.78	0.49	35.93	CheY family response regulator	NP_210_2A	WP_011322770.1:c.67G>T	WP_011322770.1:p.Glu23*
1174954	SNV	1	T	A	400	403	99.26	0.49	33.62	hydroxymethylglutaryl-CoA reductase (NADPH)	NP_242_2A	WP_011322928.1:c.1T>A	WP_011322928.1:p.Leu1Met
1213764	SNV	1	A	G	424	429	98.83	0.5	35.03	DUF5591 domain-containing protein	NP_250_6A	WP_011322970.1:c.540T>C	
1375984	SNV	1	T	C	74	153	48.37	0.17	22.47	hypothetical protein	NP_RS_14125*	WP_083761695.1:c.133A>G	WP_083761695.1:p.Met45Val
1376089	SNV	1	T	C	70	152	46.05	0.23	17.63	hypothetical protein		WP_083761695.1:c.28A>G	WP_083761695.1:p.Met10Val
1376101	SNV	1	T	C	80	165	48.48	0.24	18.66	hypothetical protein		WP_083761695.1:c.16A>G	WP_083761695.1:p.Met6Val
1376116	SNV	1	T	C	75	173	43.35	0.2	17.08	hypothetical protein		WP_083761695.1:c.1A>G	WP_083761695.1:p.Met1?
1376467	SNV	1	T	C	81	170	47.65	0.35	18.4	hypothetical protein	NP_RS_14585*	WP_158303757.1:c.68A>G	WP_158303757.1:p.Asp23Gly
1467124	SNV	1	A	C	408	410	99.51	0.48	34.31	hypothetical protein	NP_304_6A	WP_011323236.1:c.347A>C	WP_011323236.1:p.Asp116Ala
2494576	Deletion	1	C	-	477	478	99.79	0.5	34.59	VC_2705 family sodium/solute symporter	NP_513_6A	WP_049939888.1:c.677delC	WP_049939888.1:p.Ala227fs
2405308	SNV	1	T	C	111	254	43.7	0.48	34.9	putative selenium-dependent hydroxylase	NP_495_4A	WP_011324180.1:c.361A>G	WP_011324180.1:p.Asn121Asp

Blue: SNP unique to *nos::gyrB* mutant; yellow: SNP common to re-sequenced wild type and *nos::gyrB* mutant; orange: SNP unique to re-sequenced wild type.

*Original Gene Locus Tag not available.